Estuarine, Coastal and Shelf Science 277 (2022) 108056

Contents lists available at ScienceDirect

Estuarine, Coastal and Shelf Science

journal homepage: www.elsevier.com/locate/ecss

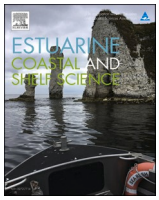

Marine heat waves and tropical cyclones - Two devastating types of coastal hazard in South-eastern Africa

D. Mawren [a,b,*], J. Hermes [a,b], C.J.C. Reason [a]

[a] Dept of Oceanography, University of Cape Town, Cape Town, South Africa
[b] South African Environmental Observation Network, Egagasini Node, Roggebaai, South Africa

A B S T R A C T

The coast of southeastern Africa is the only part of the continent to experience landfalling tropical cyclones (TCs), the most destructive and hazardous of weather systems. It is also a region which frequently experiences long-lasting marine heat waves (MHWs). Three coastal regions in southeastern Africa with high biodiversity and relatively large populations dependent on local coral reefs and artisanal fishing are analysed in terms of the characteristics of TCs and MHWs. Significantly increasing trends in MHW duration and frequency, TC heat potential and coral bleaching events are found during austral summer in all three coastal areas, with northeastern Madagascar experiencing the highest rate. The co-occurrence of TCs and MHWs in each region is also considered using a parameter-space plot of MHW intensity versus TC wind speed. A high percentage of pre-existing MHWs help strengthen TCs as they pass over the MHW region but an even higher percentage of the TCs tend to weaken or end MHWs after they both co-occur. Of the three coastal zones considered, northeastern Madagascar is more prone to landfalling severe cyclones and long-lasting MHWs. It is suggested that as the TC approaches the MHW region, the rapid increase in surface wind friction velocity, intense heat loss to the atmosphere and entrainment cooling are all important processes that determine the rate at which the MHW weakens towards its demise. TC-MHWs co-occurring together may be considered a compound extreme event. The magnitude of their impacts on the southeast African coast in recent decades highlights the need for increased monitoring and improved real-time forecasting of these devastating coastal hazards.

1. Introduction

Coastal zones have long been important to human settlements because of their diverse food sources (fish, shellfish, seaweeds etc), their moderation of regional climates with associated agricultural and ecosystem benefits, the possibility of ship-borne trade and communication with other parts of the world, and for military/political strategic reasons. As a result, many of the most important cities in the world are either on the coast or within practical access to it via navigable rivers. Coastal zones also contribute to the ocean-derived or blue economy of countries through tourism, recreational activities and, in some cases, offshore mining, oil and gas extraction. In eastern Africa, the blue economy is becoming increasingly important with Obura et al. (2017) estimating that the ocean assets of the Western Indian Ocean are valued as much as US$333.8 billion (annual output US$ 20.8 billion). In Madagascar, the World Bank (World Bank, 2020) estimated in 2018 that artisanal fisheries contributed about 7% of the gross domestic product (GDP) and directly supported the livelihoods of 1.5 million people while for Mozambique, the fisheries sector account for 4% of the GDP, supporting 5 million people.

While coastal climates are typically more moderate than inland, they can be more prone to the impacts of extreme weather events originating over the open oceans. Landfalling tropical cyclones are the most obvious example, but cut-off lows, mesoscale convective systems and atmospheric rivers have all been known to cause coastal flooding on occasion in many parts of the global coast including Africa (e.g., Singleton and Reason, 2006; Gimeno et al., 2016; Blamey et al., 2018; Morake et al., 2021). As they approach the coast, the strong winds of such storms pose significant hazards for shipping as well as often cause devastation of coastal infrastructure, coastline features, and ecosystems through storm surges.

Although Africa is the second largest continent by land area, the length of its coastline (~30,500 km) is less than the much smaller continents of Europe and Australia since it has few large bays, inlets, gulfs and coastal islands. Its coastline varies from virtually uninhabited (e.g., Namibia, Mauritania) to hosting some of the largest cities in the world (e.g., Lagos, Cairo); over 60 million people live within 100 km from the South West Indian Ocean (SWIO) coast. Here focus is placed on the southeastern African coast (i.e. Mozambique Channel region) which includes Madagascar (the world's fourth largest island by land area), Mozambique (African country with the longest coastline) and small island developing states such as Comoros. The Mozambique Channel itself

* Corresponding author. Dept of Oceanography, University of Cape Town, Cape Town, South Africa.
E-mail address: daneejamawren@gmail.com (D. Mawren).

https://doi.org/10.1016/j.ecss.2022.108056
Received 31 August 2021; Received in revised form 18 July 2022; Accepted 22 August 2022
Available online 28 August 2022

is of great interest oceanographically (Mawren et al., 2022) - it is dominated by mesoscale southward propagating eddies (Backeberg and Reason, 2010; Ridderinkhof et al., 2013; Halo et al., 2014) which help promote biological productivity (Mikaelyan et al., 2020), contribute to the intensification/weakening of tropical cyclones (Mawren and Reason, 2017; 2020), modulate marine heat wave intensity (Mawren et al., 2022), and for being one of the three sources of the Agulhas Current, the largest western boundary current in the world (Lutjeharms, 2006). This region is chosen for study because it is the only part of the African coast to experience tropical cyclones, and is often impacted by marine heat waves, two prominent examples of coastal hazards.

The vulnerability of communities living in this coastal zone exposed to hazards like landfalling tropical cyclones is increasing due to large population growth rates, relatively weak and undeveloped economies, and the impacts of global warming (World Bank, 2017). However, due to recent offshore oil and gas discoveries in the Mozambique Channel, the region may assume increasing economic importance within Africa. A significant challenge will be to exploit these resources to the benefit of the local populations without significantly damaging the high biodiversity and tourism potential there. Currently, Mozambique and Madagascar are some of the world's poorest countries as well as the most vulnerable and least prepared for climate change (WFP, 2021). For example, in 2019, Mozambique was rated as the fifth most affected country world-wide by the impacts of extreme weather events (Eckstein et al., 2021).

The broader SWIO region, and particularly the Mozambique Channel (Fig. 1a), supports pristine ecosystems, high biological diversity, high endemism, and endangered species as well as being home to the second most biodiverse area for coral species in the Indo-Pacific (Obura, 2012; Pereira et al., 2014). By disrupting the locations and health of available fish stocks which so many people in these countries depend on, intense and long-lasting marine heat waves in this region can have very significant socio-economic impacts. Mawren et al. (2022) showed that the frequency and intensity of marine heat waves in the coastal region off southwestern Madagascar have significantly increased during 1982–2019. More frequent and intense marine heat waves pose severe threats to the ongoing viability of coral reefs and associated organisms (Hughes et al., 2003; Sheppard, 2003; Graham et al., 2006; Wilson et al., 2006), causing significant risks to the many coastal communities in the region dependent on these ecosystems. While no studies to date have estimated the socio-economic impacts of marine heat waves in the SWIO region, elsewhere in the world they have led to economic losses of many millions of dollars (Mills et al., 2013; Cavole et al., 2016) due to substantial shifts in the distributions of important stocks (e.g. Walker et al., 2020) or mass mortality events. Particularly important coastal SWIO ecosystems are mangrove forests, sea grasses and coral reefs. The former help mitigate against the impacts of tropical storms by reducing coastal erosion associated with heavy winds and direct exposure to storm waves as well as providing valuable ecosystem services for the wellbeing of coastal communities. However, intense tropical cyclones can also reduce viable mangrove extent after landfall (Paling et al., 2008) as well as damage coral reefs. Coral reefs in this region are often prone to significant damage from marine heat waves as well as from warming during anomalous seasons (such as the 1997/98 El Niño) or from climate change (Obura et al., 2012).

While the Madagascan coast has long been impacted by landfalling tropical cyclones, in the last two decades Mozambique has suffered very heavy loss of life and severe damage from several landfalling intense cyclones such as Eline in 2000 (Reason and Keibel, 2004), Japhet in 2003 (Mavume et al., 2009), Favio in 2007 (Klinman and Reason, 2008), Idai and Kenneth in 2019 (Mawren et al., 2020). Intense rainfall, extreme winds, highly energetic waves, and storm surges are the tropical cyclone hazards impacting this coast leading to deaths and destruction. For example, during the 2018–2019 season when Idai and Kenneth occurred, the impacts included over 1380 deaths and about 2.3 billion USD worth of infrastructural damage.

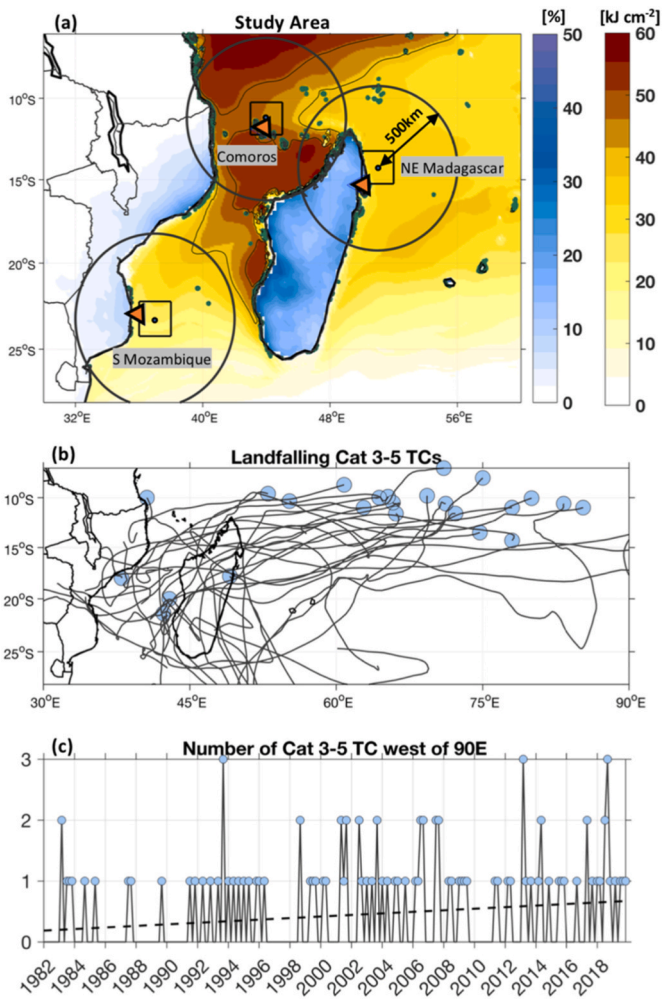

Fig. 1. **(a)** Mean tropical cyclone heat potential (TCHP, kJ cm^{-2}; computed from GLORYS12V1 product from 1993 to 2019) averaged during tropical cyclone season (November–April) highlighting 3 coastal areas of interest: Comoros islands, North East (NE) Madagascar and South Central Mozambique. Black contours show TCHP values of 40 kJcm^{-2} and above. Blue colorbar over land represents the percentage contribution of annual rainfall from tropical cyclones (including tropical storms) between November through to April computed from daily CHIRPS data over the period 1981–2019. Green shading along coastal areas represents the distribution of warm water coral reefs (UNEP-WCMC et al., 2018). Coral bleaching hotspot values (represented by orange triangles) were extracted at 3 virtual stations (Inhambane (36.0°E, 23°S), Comoros (43.8°E, 11.9°S) and NE Madagascar (49.90°E, 15.3°S); NOAA Coral Reef Watch, 2018). Marine heatwave metrics are analysed near virtual stations within 2°x2° boxes (Comoros (10.25–12.25°S; 43.0–45.0°E), NE Madagascar (13.25–15.25°S; 50.0–52°E) and southern Mozambique (22.25–24.25°S; 36.0–38.0°E)). Large circles include all tropical storms and cyclones that cross within a 500 km radius from the centre of the boxes. **(b)** All tropical cyclones (maximum sustained winds exceeding 90 knots) that made landfall during austral summer (November–April) in the Southwest Indian Ocean between 1982 and 2019. Blue dots are where tropical cyclones of Category 3–5 are formed respectively. **(c)** Time series (monthly count from November to April; for e.g., Year, 2018 starts in November 2018 and ends in April 2019) of tropical cyclones of Category 3–5 (Intense to very Intense cyclones) in SWIO i.e. east of 90°E. The dashed black lines represent the linear trend. (Trend is statistically significant, $p < 0.05$). (For interpretation of the references to color in this figure legend, the reader is referred to the Web version of this article.)

With climate model projections indicating an increase in the frequency and intensity of severe tropical cyclones, and increasing ocean temperatures in the near future (INGC, 2009; Arndt et al., 2010; IPCC et al., 2013; 2021) and hence MHWs (Hobday et al., 2016; Oliver et al., 2017, 2018, 2019), coastal communities in Mozambique, Madagascar and neighbouring islands need to adapt to reduce the severe impacts of these extreme events on their livelihood (Hahn et al., 2009; Osbahr et al., 2010; Artur and Hilhorst, 2012).

For coastal hazard management and mitigation, important questions arise about the co-occurrence of MWHs with TCs leading to compound extreme events in a particular coastal location and whether they may influence the characteristics or lifespan of each other. For example, since tropical cyclogenesis needs SST >26 °C (Pielke, 2013) and storms can intensify as temperatures warm further, a pre-existing marine heat wave may make conditions more favourable for these systems. On the other hand, a tropical cyclone tracking over a MHW region may extract heat from the ocean surface and may in turn terminate the marine heat wave (Rathore et al., 2022).

Thus, the objectives here are to examine the characteristics of tropical cyclones and marine heat waves impacting the coast of southeastern Africa and how they may interact with each other. To do so, focus is placed on three coastal regions in southeastern Africa, namely, south-central Mozambique, northeastern Madagascar, and the Comoros islands, all characterized by coral reefs and high biodiversity and particularly sensitive to tropical cyclone (TC) and marine heat wave (MHW) hazards (Fig. 1a).

2. Data and methods

The three coastal regions focussed on in this study are centred near South-central Mozambique/Inhambane (23°S, 36.0°E), Comoros (11.9°S, 43.8°E) and northeastern Madagascar (15.3°S; 49.9°E) and at these coordinates, virtual stations are defined (Fig. 1a) to assess coral bleaching hotspots.

NOAA defines a coral bleaching hotspot when the SST in a particular area exceeds the maximum monthly mean SST by at least 1 °C. Regions with hotspot values of 1 °C or more imply that corals there are experiencing heat stress leading to bleaching. In this study, the NOAA Coral Reef Watch (CRW) version 3.1 (NOAA Coral Reef Watch, 2018) operational global satellite coral bleaching heat stress monitoring product at 5-km resolution produced daily in near real-time is used for the period 1986–2020.

Daily optimally interpolated sea surface temperature (OI SST) V2 high resolution (1/4°) gridded data (Banzon et al., 2016) were used to detect MHW occurrences. A MHW is defined as a discrete, prolonged, anomalously warm water event with clear start and end date, with a duration of at least five consecutive days for which the temperature is above the seasonally varying 90th percentile (the threshold) for that time of the year (Hobday et al., 2016). Two successive events with a break of 2 days or less between them were considered a single continuous event. Given that a warm event has to last at least 5 days to be classified as a MHW and that the upper ocean temperature responds to surface heat flux changes on time scales of hours to a day or so, this 2 day break is appropriate. The seasonally varying mean and the 90th percentile threshold were calculated for each day of the year using daily SST data for a climatological period of 1983–2012 (the same period as Hobday et al., 2016; Oliver et al., 2021) and within an 11-day window centred on the day, which were then smoothed using a 31-day moving window. The 11-day sample window size was chosen since the minimum duration of a MHW is 5 days and to ensure sample sizes were sufficient for the estimation of means and percentiles. Furthermore, by using seasonally varying thresholds, rather than a fixed mean annual threshold, this methodology allows for detection of MHWs at any time of the year.

The following MHW metrics are determined for January 1, 1982 to December 31, 2020: duration (the time between the start and end dates), mean intensity (the average temperature anomaly over the duration of the event), frequency (number of events in a year or a season) and cumulative intensity (the integrated SST anomaly over the duration of the event). These metrics (Hobday et al., 2018) are available as software modules in MATLAB (https://github.com/ZijieZhaoMMHW/m_ mhw1.0). The m_mhw toolbox is designed 1) to determine spatial MHWs according to the definition provided in Hobday et al. (2016) and marine cold spells (MCSs) introduced in Schlegel et al. (2017); 2) to visualize MHW/MCS event in a particular location during a period; 3) to explore the mean states and trends of MHW metrics, such as what have done in Oliver et al. (2018). MHWs metrics are analysed for the austral summer, i.e. tropical cyclone season from November through to April in 2°x2° boxes near North-East of Madagascar (13.25–15.25°S; 50–52°E), Comoros (10.25–12.25°S; 43–45°E) and south-central Mozambique (22.25–24.25°S; 36–38°E). MHW intensities are characterized as moderate (1–2x, Category I), strong (2–3x, Category II), severe (3–4x, Category III) and extreme (>4x, Category IV), where 'x' refers to the multiple of the temperature difference between the climatological mean and the climatological 90th percentile at a given location (Hobday et al., 2018).

The International Best Track Archive for Climate Stewardship (IBTrACS) data set (Knapp et al., 2010, 2018) (1982–2020) is used to examine tropical cyclone (TC) numbers, intensity, and tracks occurring in the SWIO. These data include the position of the TC centre, landfalling TCs, and 10 min average maximum sustained wind speed every 3 h. The classification of tropical cyclone intensity is defined according to its wind speed and varies depending on the regional ocean basins. In this study, a tropical storm is defined as a system with maximum sustained winds of 63 kts, tropical cyclone of category 1–2 is estimated to have maximum sustained winds of 64–89 kts, Category 3–4 tropical cyclone (Intense tropical cyclone) has maximum sustained winds of 90–115 kts and Category 5 tropical cyclone (Very Intense tropical cyclone) is the highest category on the SWIO tropical cyclone scale with winds exceeding 115 kts.

In previous studies, the 95th percentile of all the samples of 24-hr changes in maximum sustained wind speed ($\Delta V_{24} = V_{+24h} - V_{0h}$) for TCs in an ocean basin was often used as the threshold to define rapid intensification (RI; Kaplan and DeMaria, 2003). In this study, the 95th percentile of all ΔV_{24} samples of TCs during 1982–2020 in all three coastal areas is 30 knots, where values exceeding 30 knots within 24 h are defined as RI events.

The accumulated rainfall contributed by tropical cyclones was calculated from daily Climate Hazards Group InfraRed Precipitation with Station Data (CHIRPS) which is available over land only from 1981 to near present at a resolution of 0.05° (Funk et al., 2014). The total TC rainfall is defined using the 500 km radius threshold as per many other studies (Larson et al., 2005; Jiang et al., 2011; Matyas, 2013, 2014) to ensure that the TC eyewall, inner and outer rainbands are included. The daily position (longitude and latitude) of the cyclone is extracted from IBTrACS and daily rainfall is sourced from CHIRPS. The daily precipitation within a 500 km area around the center of the cyclone is estimated and summed for all the cyclones crossing the SWIO during TC season (November through to April) 1981–2019.

In this study, the co-occurrence of TCs and MHWs is defined as the number of instances (in days) that a cyclone passes within 500 km of a region (large circles in Fig. 1a) currently experiencing a MHW. This methodology is illustrated in supplementary Figure A1a-c, indicating all TCs (including storms) within 500 km from each study box (tracks in blue), regardless of whether they encounter a MHW. To obtain the days where both extreme events co-occur, supplementary Figure A1 d-f illustrate daily MHW intensity averaged in each 2°x2° box (in grey) over the period 1982–2020 overlaid with co-occurring TCs or days that a cyclone is within the MHW region (in blue dots).

Surface wind stress τ is computed from zonal and meridional winds at 10 m above sea level from ERA5 reanalysis data, at a horizontal resolution of 80 km (https://cds.climate.copernicus.eu/cdsapp#!/datas

et/reanalysis-era5-single-levels?tab=overview) to obtain the friction velocity ($u_* = \sqrt{\tau/\rho}$, where ρ is the density of seawater; Niiler, 1977; Foltz et al., 2010). To compute the total air-sea heat flux, hourly surface sensible heat flux, surface latent heat flux, and surface radiation component (short and long-wave radiation) data were extracted from ERA5 and averaged over the North-East Madagascar, Comoros, and South-central Mozambique 2°x2° grid boxes defined above (https://cds.climate.copernicus.eu/cdsapp#!/dataset/reanalysis-era5-single-levels?tab=form).

Daily subsurface temperature data were extracted from the GLORYS12V1 product for the region between January 1993–December 2019 to compute the TCHP, an important parameter for TC intensification (Lin et al., 2013; Sadhuram et al., 2010; Shay et al., 2000). The GLORYS12V1 product is a CMES global ocean eddy-resolving (1/12 deg horizontal resolution and 50 vertical levels) reanalysis (https://doi.org/10.48670/moi-00021). TCHP is defined as the heat content relative to 26 °C isotherm and is computed as follows:

$$\mathrm{TCHP} = \rho C_p \sum \Delta T \Delta Z$$

where ρ is density of the sea water, C_p is the specific heat capacity at constant pressure, ΔT is the temperature difference between sea temperature across each level and 26 °C, and ΔZ is the thickness of each layer between the sea surface and depth of the 26° isotherm. TCHP has previously been shown to be important for TC generation and intensification (Shay et al., 2000; Wada and Usui, 2007).

Another ocean parameter that can favour TC intensification is barrier layer thickness (BLT) since it reduces the storm-induced cooling feedback with the upper ocean (Wang et al., 2011; Balaguru et al., 2012). BLT is defined as the difference between isothermal layer and mixed layer and intensification can occur if the BLT is at least 10 m in magnitude (Balaguru et al., 2012).

An estimate of the mixed layer depth was made using a threshold criterion of 0.2 °C from the temperature closest to the surface (de Boyer Montégut et al., 2004).

The upper ocean *cooling* is primarily controlled by the *entrainment* of cold water from the thermocline into the mixed layer through vertical mixing. The entrainment velocity, W_e is calculated as follows:

$$W_e = \frac{\partial h}{\partial t} + u_{-h}\frac{\partial h}{\partial x} + v_{-h}\frac{\partial h}{\partial y} + w_{-h} \quad (1)$$

$$\mathrm{Entrainmentheatflux} = \rho C_p W_e \Delta T \quad (2)$$

Where u_{-h}, v_{-h} denote the horizontal components of velocity at the base of the mixed layer, w_{-h} is the vertical velocity at the base of the mixed layer and ΔT is the difference between the average mixed layer temperature and the temperature at the base of the mixed layer. ρC_p are the mean density and specific capacity of sea water respectively. Due to the unavailability of vertical velocity data (term 4 in equation (1)), the entrainment velocity is only estimate from the first three terms on the RHS of equation (1).

The significance of the linear trends was evaluated using a two-tailed Student's *t*-test at 95% throughout the manuscript.

3. Results

3.1. Tropical cyclone-rainfall contribution and ocean influences

In addition to showing the southeastern African coastal area and the three virtual stations studied in relation to the coral reefs, Fig. 1a indicates the climatological TCHP from November through to April in the neighbouring ocean as well as the percentage of rainfall over land that results from tropical cyclones on average. The entire region experiences average SST of at least 26 °C during the November–April season (Mawren et al., 2022) and TCHP values exceed 50–60 kJcm^{-2} in the northern Mozambique Channel. These oceanic conditions are conducive for TC genesis and intensification, provided that atmospheric conditions are also favourable.

During this season, North-East and South-West Madagascar receive the highest percentage of summer rainfall associated from TCs (between 40 and 50%) due to a higher density of TCs of Category 3–5 crossing the southeastern Mozambique Channel and Madagascar, contributing to a lot of rainfall there (Fig. 1b). Mozambique however receives lesser rainfall due to fewer landfalling storms than NE Madagascar (Table 1). North coastal Mozambique receives up to 30% of its rain from TCs whereas in the south-central Mozambican coastal zone of interest here, the contribution is 10–20%. Nevertheless, in some summers individual TCs have made much larger contributions to rainfall causing loss of life and damage. For instance, in the past two decades, three intense cyclones, TC Eline in 2000, TC Japhet in 2003 and TC Idai in 2019, tracked westward through Mozambique and eastern Zimbabwe, contributing to 10% of summer rainfall and severe flooding inland (Mukwenha et al., 2021). Comoros islands have also been impacted by two of the most intense TCs ever recorded in the Mozambique Channel in recent years (Hellen in 2014 and Kenneth in 2019, Mawren et al., 2020).

Fig. 1b shows the tracks of intense TCs (categories 3–5) that have made landfall in the region between 1982 and 2020, including their genesis locations (blue circles). It is important to note that this is only a fraction of the total number of TCs that have affected and contributed to rainfall in the coastal zones (South-Central Mozambique, Comoros and North-East Madagascar in Fig. 1a). From Fig. 1b, it is apparent that Madagascar (North-East Madagascar in particular) more frequently experiences landfalling severe cyclones than does South-Central Mozambique and Comoros. In terms of total tropical storms making landfall, northeastern Madagascar is also more impacted (Table 1), with twice (four times) as many as South Mozambique (Comoros). However, for TCs passing within 500 km of the virtual station, Table 1 shows that northeastern Madagascar experiences about twice the number than do the other two stations.

Table 1
TCHP trends (1993–2019), MHW metrics (Frequency, Intensity, Duration and Cumulative Intensity) trends (1982–2019) computed annually (in bold) and during austral summer (November through to April) in study box: NE Madagascar, Comoros, and South-central Mozambique. Number of tropical storms (including tropical cyclones) between 1982 and 2019 that crossed within 500 km from each study regions: NE Madagascar, Comoros, and South-central Mozambique.

	NE Madagascar	Comoros	South-central Mozambique
MHW intensity trend (°C. decade^{-1})	**- 0.027**	**- 0.036**	**+ 0.012**
	+0.055	- 0.013	+0.049
MHW frequency trend (events. decade^{-1})	**+ 1.47**	**+ 1.16**	**+ 1.29**
	+0.45	+0.32	+0.65
MHW duration trend (days. decade^{-1})	**+ 2.76**	**+ 1.50**	**+ 0.042**
	+2.82	+1.05	+1.04
MHW cumulative intensity trend (°Cdays.decade^{-1})	**+ 2.94**	**+ 1.32**	**+ 0.06**
	+3.42	+1.07	+1.44
TCHP trend (kJcm^{-2}per decade)	+8.61	+7.52	+3.28
Number of TCs (including TS) within 500 km of region	122	55	68
Number of Cat 1 – 2 cyclones within 500 km of region	22	11	13
Number of Cat 3 – 4 cyclones within 500 km of region	26	8	10
Number of Cat 5 cyclones within 500 km of region	8	4	2
Number of Landfalling TS (including TCs)	43	12	20
Number of landfalling TCs			
(Cat 1–2)	11	3	2
(Cat 3–4)	11	3	6
(Cat 5)	3	0	1

3.2. Tendencies and variability during austral summer

For the region west of 90°E, Fig. 1c indicates that whereas more severe TCs (categories 3–5) have occurred since 1999 than during 1982–1998, some individual months (March 1994, December 2013, and March 2019) have recorded up to 3 intense SWIO TCs. Over the whole period 1982–2020, an increasing trend of 0.21 ITCs per decade (statistically significant at 95%) is observed in the region, along with an increasing trend of severe TC days over the broader SWIO region (Malan et al., 2013). In addition, this broader ocean area is warming faster than many other areas in the global ocean (IPCC et al., 2021) leading to increasing tendency in TCHP. For the three coastal zones studied here,

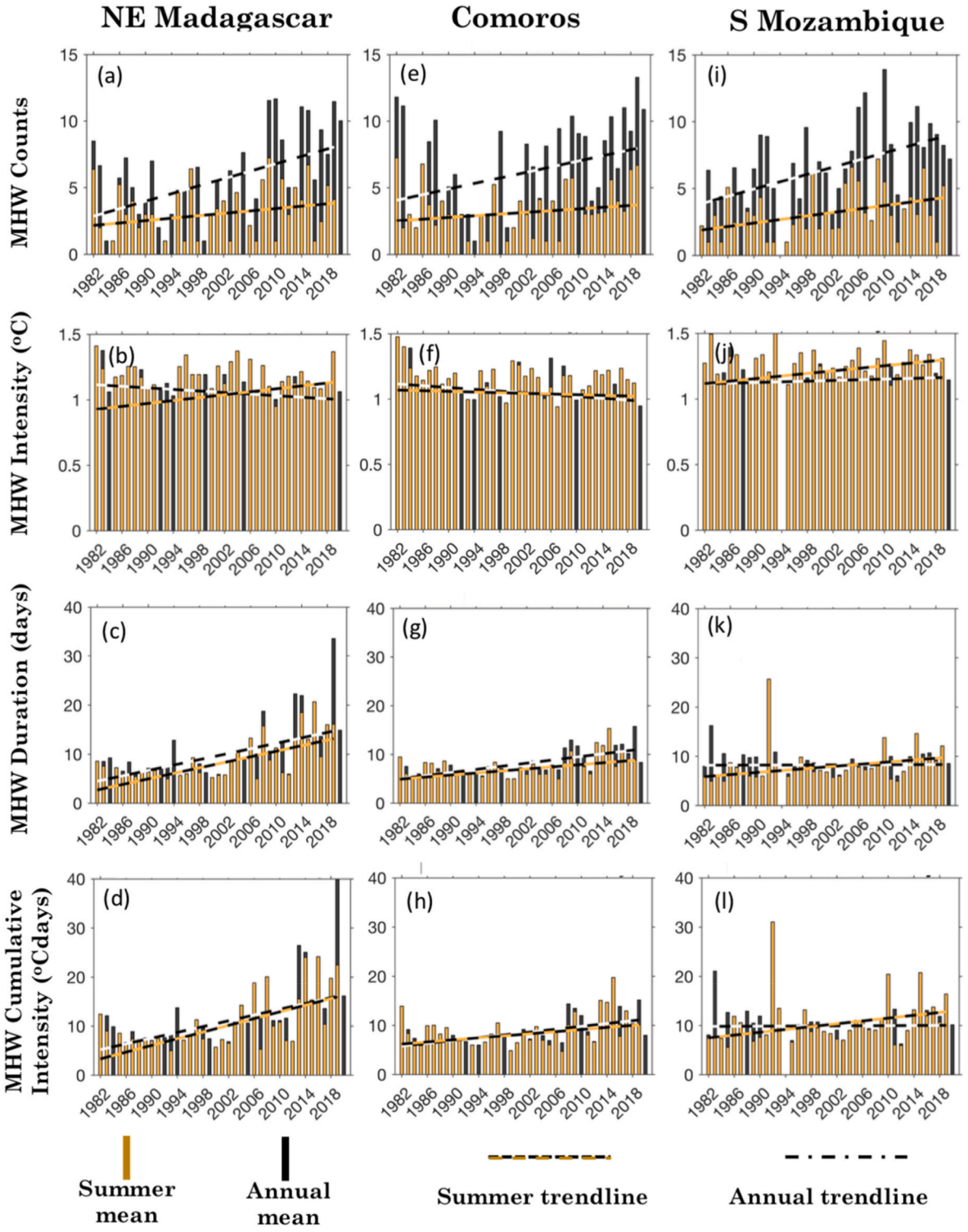

Fig. 2. Time series and trends of mean MHW metrics computed annually (in black) and for summer (in brown) months (November–April for e.g., The year 2006 starts in November 2006 and ends in April 2007) (a) counts, (b) mean intensity (°C), (c) mean duration (days), (d) mean cumulative intensity (°C days) averaged over box NE Madagascar, (e–h) Comoros, and (i–l) South-central Mozambique. All trends are statistically significant at 95%. (For interpretation of the references to color in this figure legend, the reader is referred to the Web version of this article.)

Table 1 shows that each has a significantly increasing TCHP trend with about twice as fast in the northern Mozambique Channel region (Comoros; 7.5 kJcm^{-2}) and NE Madagascar (8.6 kJcm^{-2}) than off the SE coast of Mozambique. These results imply that if the subsurface ocean temperature continue to rise, TCs tracking over these three zones are more likely to intensify there, assuming that the atmospheric environment remains favourable.

As ocean temperature increases in the SWIO region, prolonged and intermittent MHWs are more likely to occur (Mawren et al., 2021) and can be a threat to local ecosystems and economies. Fig. 2 shows statistically significant trends in MHW metrics at the three coastal boxes computed annually and during austral summer. The latter is of crucial importance for countries bordering the Mozambique Channel due to frequent and intense tropical cyclones and associated coastal impacts. The actual increases per decade and the interannual variability of each of MHW metric (duration, frequency, intensity and cumulative intensity) are given in Table 1 and Fig. 2 respectively. NE Madagascar shows the most prominent trend in MHW frequency, duration and cumulative intensity annually compared to the other study areas (Table 1, Fig. 2a,c,d). The increasing trend in the occurrence of MHWs NE of Madagascar is about 1.47 MHW events per decade ($p < 0.05$; Table 1 in bold), which is in agreement with the western Indian Ocean region (Saranya et al., 2022). However, the intensity of MHWs exhibit a decreasing trend NE Madagascar (annually, Fig. 2b) and in the northern Mozambique Channel, near Comoros (annually and during summer, Fig. 2f), despite TCHP increase (Table 1). According to a recent study by Gao et al. (2022), as MHWs become more frequent and prolonged, the extended MHW days may decrease the averaged intensity of temperature anomalies for MHWs, resulting in a negative trend in MHW intensity. Southeastern Mozambique on the other hand shows a positive increase in MHW intensity (both annually and during austral summer, Fig. 2j) and displays the highest MHW frequency trend (0.65 MHWs per decade; $p < 0.05$, Fig. 2i) during summer compared to the other study areas. Cumulative intensity during austral summer is increasing at a faster rate in northeastern Madagascar (3.4°Cdays per decade; $p < 0.05$) than Comoros (1.1°Cdays per decade; $p < 0.05$) and southeastern Mozambique (1.4°Cdays per decade; $p < 0.05$). With most coastal zones experiencing significant increases in MHW trends during summer, warm water coral reefs (green shading in Fig. 1a) are becoming more under threat as they are largely dependent on the physical changes occurring at and near the surface of the ocean.

Since summer months in almost all years show higher cumulative intensity than annually (Fig. 2d, h, l), coral reefs may be more vulnerable during this season. Fig. 3 plots Coral bleaching hotspot data during the summer to determine whether coral reefs in the three coastal zones are exceeding the bleaching threshold more often in the more recent years of the record. A statistically significant increasing trend in coral bleaching cases is observed in each region. Again, the trend is faster in the northeastern Madagascar box than for southeastern Mozambique and the Comoros. The warming rate indicated by coral bleaching hotspot for northeastern Madagascar is not only two times as fast (0.11°Cdecade^{-1}) than the other two regions, Comoros (0.06 °Cdecade^{-1}) and southeastern Mozambique (0.05°Cdecade^{-1}), but it also shows a series of frequent and intense of coral bleaching events (red filled circles in Fig. 3) after the first global bleaching event in 1998. Other prominent bleaching years for the western Indian Ocean were 2016 and late summer 2010, with widespread coral bleaching and mortality in the northern Mozambique Channel (Eriksson et al., 2012; Obura et al., 2018). Although some of the main bleaching events coincide with strong El Niño events (1998, 2010, 2016 summers) not all (e.g. 2021) do. This nonlinear relationship may result because the Mozambique Channel region does not show a consistent SST signal during ENSO events (Reason et al., 2000; Mawren et al., 2021).

Strong MHWs in coral regions are likely to result in bleaching there. For instance, the region south-central of Mozambique (Fig. 3a) experienced coral bleaching during austral summers 2010–2011, 2015–2016

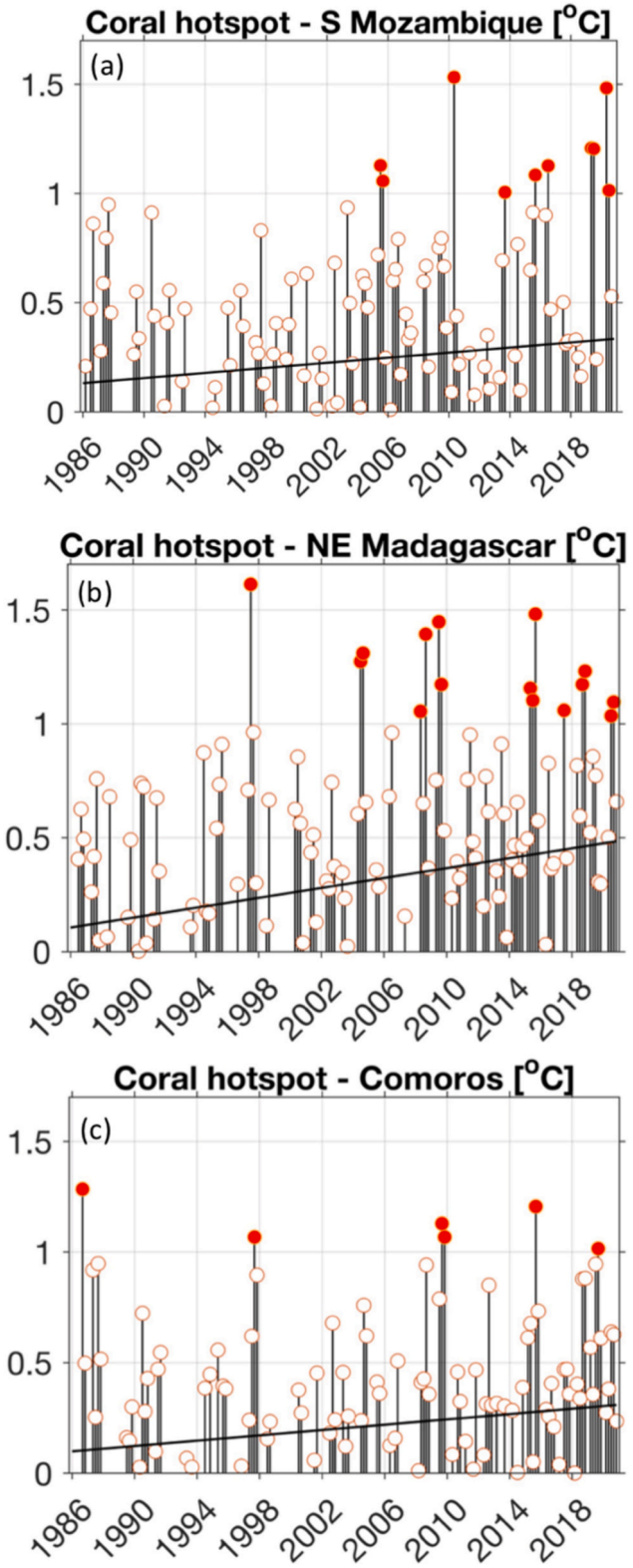

Fig. 3. Coral bleaching Hotspot data (SST exceeding maximum monthly mean (MMM), °C) during austral summer observed by NOAA's polar orbiting satellites from 1985 to 2021 near (a) South-central Mozambique (near Inhambane), (b) NE Madagascar and (c) Comoros. Hotspot values exceeding 1 °C highlights areas (red filled circles) are above the bleaching threshold and implies that corals in those areas are experiencing heat stress that leads to bleaching. All trends are significant at 95%, determined by the Student's *t*-test. (For interpretation of the references to color in this figure legend, the reader is referred to the Web version of this article.)

and 2019–2020 due to large increases in MHW occurrences and long-lasting MHWs (Fig. 2i,k). The string of coral bleaching events NE of Madagascar (Fig. 3b) in the recent decade, appear to be linked with either frequent and intense MHWs or long-lasting MHWs. Following the recent extreme thermal stress in the Mozambique Channel in January–February 2021 (a maximum of 10–15 Degree-Heating-Weeks (DHW) in Inhambane), further south along the Agulhas current, extreme temperatures in February–March 2021 caused widespread bleaching, resulting in significant fish mortality (Department of Forestry, 2021). The impacts of MHWs on other marine ecosystems such as seagrasses and mangroves in SWIO region remain under-reported. According to George (2019), seagrasses in the SWIO are at risk as they are currently living in an environment where ambient water temperatures frequently reach or exceed their threshold levels during summer. Amone-Mabuto et al. (2017), showed that over a 21-year period (1993–2013) the most extensive decline in seagrasses in Inhambane bay, Mozambique occurred during 1998–2001 which is when there were frequent occurrences of MHWs (Fig. 2). In addition, the strong winds and heavy rains associated with TC Eline played a role.

3.3. TC MHW co-occurrences

Exposure to extreme events in coastal zones is a major concern as it is often exacerbated by climate change, population growth and the likelihood of compound events coinciding. Comparatively to a severe drought in a particular region might occur at the same time as a devastating bush fire there, leading to a compound extreme event with severe impacts, marine ecosystems might experience a compound event which includes a TC tracking through a location that is already in a MHW situation. In this section, the co-occurrence of MHWs and tropical cyclones are analysed over the period 1982–2020 in all three coastal zones, NE Madagascar, Comoros, and south-central Mozambique.

A visual representation of TC-MHW co-occurrences in Figs. 4–6 illustrates the onset (black dot) and cessation (yellow dot) months of

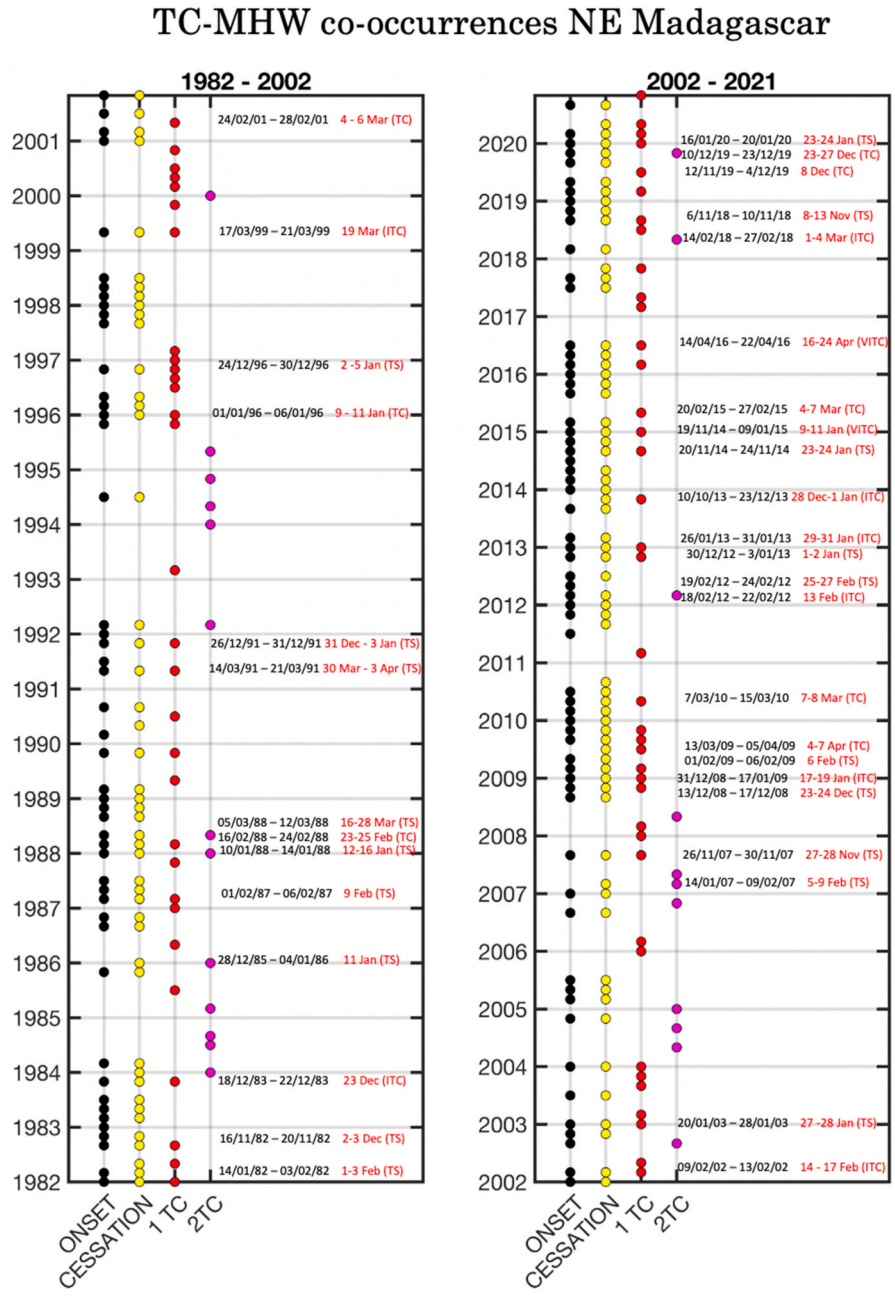

Fig. 4. Onset (Black dots) and Cessation month (yellow dots) of monthly MHW events observed during summer 1982–2020 (Y-axis only shows half of the year, i.e., January to April 1982, followed by November to December 1982) northeast of Madagascar in box (13.25–15.25°S; 50–52°E) with tropical cyclones (including tropical storms) (red and magenta dots) that crossed within 500 km from the centre of the MHW box. 1 TC and 2 TC are the number of cyclones (including tropical storms) observed within 500 km from MHW box during each month. The duration of the MHW event (text in black) coinciding with the date of a passing cyclone (text in red) is also noted. (For interpretation of the references to color in this figure legend, the reader is referred to the Web version of this article.)

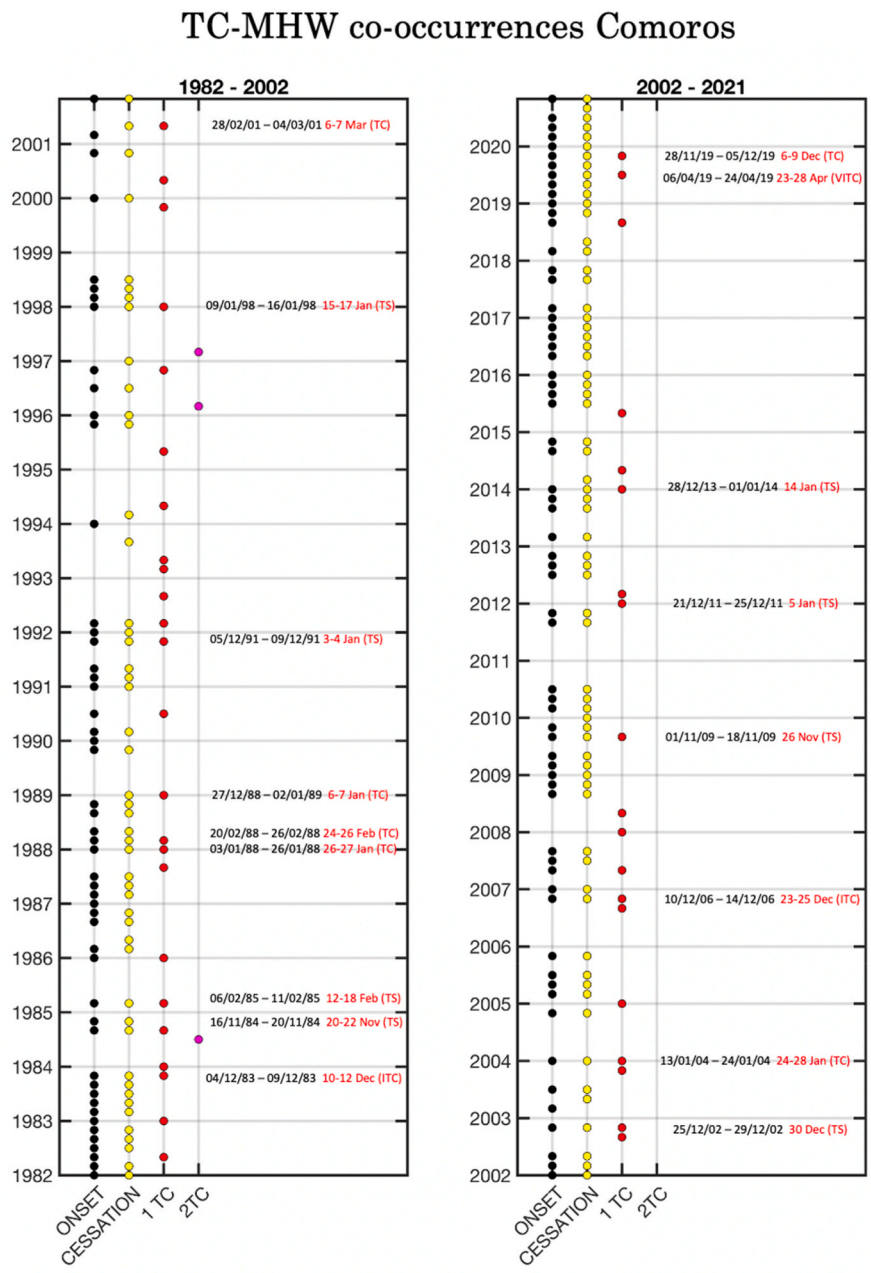

Fig. 5. Onset (Black dots) and Cessation month (yellow dots) of monthly MHW events observed during summer 1982–2020 (Y-axis only shows half of the year, i.e., January to April 1982, followed by November to December 1982) in Comoros in box (10.25–12.25°S; 43–45°E) with tropical cyclones (including tropical storms) (red and magenta dots) that crossed within 500 km from the centre of the MHW box. 1 TC and 2 TC are the number of cyclones (including tropical storms) observed within 500 km from MHW box during each month. The duration of the MHW event (text in black) coinciding with the dates of a passing cyclone (text in red) is also noted. (For interpretation of the references to color in this figure legend, the reader is referred to the Web version of this article.)

MHWs in each coastal zone along with the number of TCs (and their categories) encountering the MHW region during each summer month (red and pink dots are months that experience 1 or more cyclone respectively). Labelled dates in black highlight the actual MHW dates and those in red are the days when both MHWs and TCs co-occur. Using the dates in red only (TC-MHW co-occurrences), Fig. 7 shows tropical cyclone winds (x-axis) relative to MHW intensity (y-axis) during TC-MHW co-occurrence in the regions northeast of Madagascar, Comoros, and south-central Mozambique.

Note that there are several MHW events without a TC since the former only requires anomalously warm SST whereas, in addition to SST >26 °C, TCs also need favourable atmospheric conditions to be maintained (such as weak vertical wind shear, pre-existing sufficiently moist and unstable air mass) for a pre-existing easterly disturbance to strengthen to and beyond Tropical Storm status. There are also a few cases when TCs occur but no MHW since SST only needs to reach 26 °C for cyclogenesis to be possible whereas it needs to be considerably warmer (exceeding the 90th percentile threshold in time and space) for a MHW event to occur. Note that climatological SST is at least 26 °C in the three regions throughout October–April (Mawren et al., 2022). The number of TC-MHW co-occurrences are greater in northeast of Madagascar than the other two regions due to the larger portion of TCs impacting Madagascar (Table 2) although when expressed as a percentage both northeast Madagascar and south Mozambique show around 13% of MHWs co-occurring with a TC.

3.3.1. *MHW as a pre-conditioning factor for TC intensification*

To consider the effect of MHW on TCs, Fig. 7 shows how the magnitude of TC winds changes when encountering a MHW. Before encountering the MHW region, TCs have significantly lower TC wind speed (mostly of Tropical Storm intensity, not shown), but as TCs encounter the MHW area, they gain energy from the warmer ocean along their trajectory paths and intensify further.

Out of the 426 days that TCs spent within 500 km of the NE

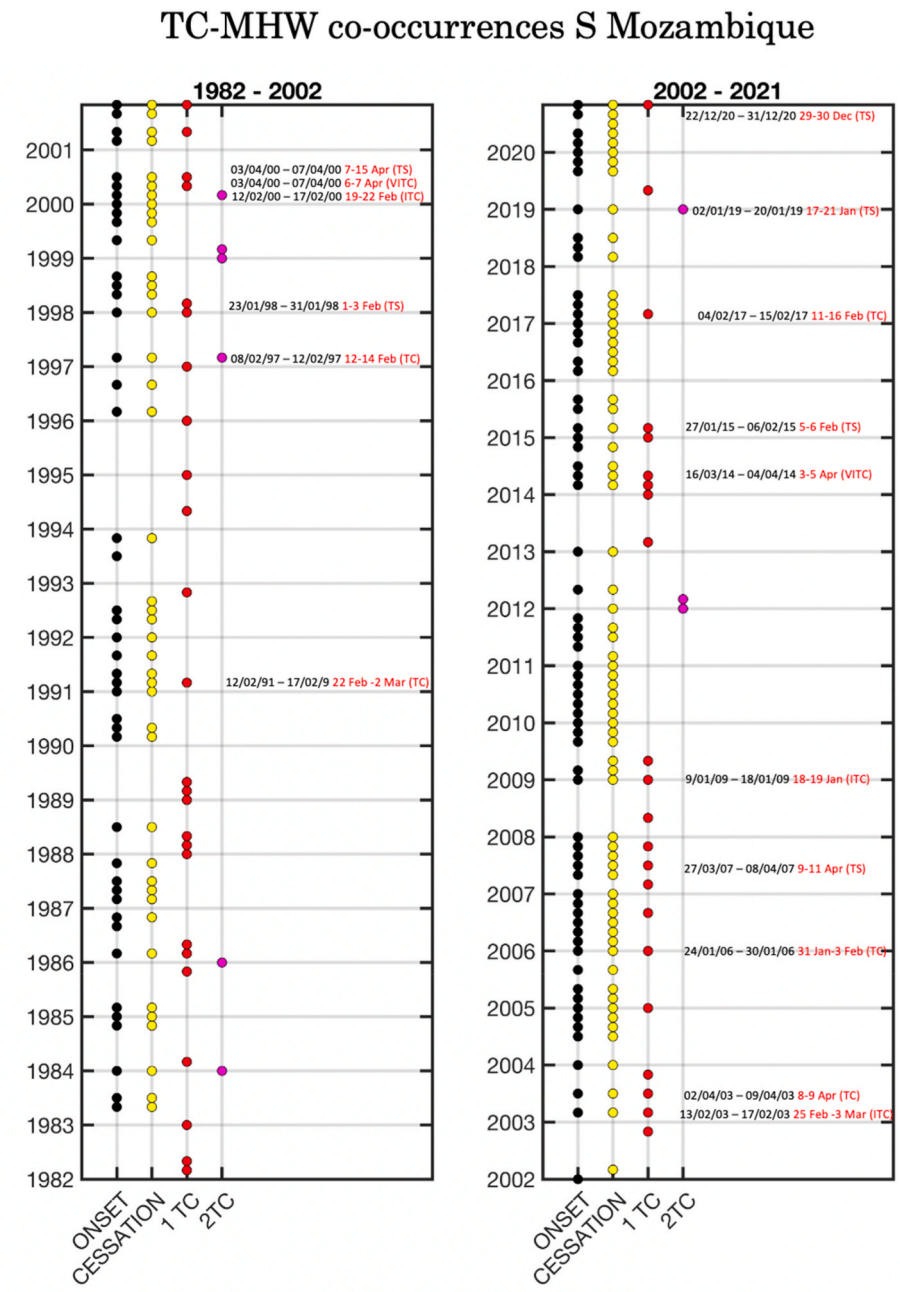

Fig. 6. Onset (Black dots) and Cessation month (yellow dots) of monthly MHW events observed during summer 1982–2020 (Y-axis only shows half of the year, i.e., January to April 1982, followed by November to December 1982) off the south-central coast of Mozambique in box (22.25–24.25°S; 36–38°E) with tropical cyclones (including tropical storms) (red and magenta dots) that crossed within 500 km from the centre of the MHW box. 1 TC and 2 TC are the number of cyclones (including tropical storms) observed within 500 km from MHW box during each month. The duration of the MHW event (text in black) coinciding with the date of a passing cyclone (text in red) is also noted. (For interpretation of the references to color in this figure legend, the reader is referred to the Web version of this article.)

Madagascan region over the period 1982–2020, 59 days show co-occurrence with a MHW there (Table 2, Figs. 4 and 7 a, A.1), roughly 13% of the time. NE Madagascar also indicates that about 72% of TCs that co-occur with a MHW (~48% of TC-MHW days), undergo further intensification (Table 2). Fig. 7a indicates a large increase in TC wind intensity as these storms pass over the MHW with about 8 instances reaching TC status (4 instances of intense and very intense TCs), including one case of rapid intensification, VITC Bansi (Table 2). Although several TCs do not show TC intensification as they pass over the MHW (open circles in Fig. 7), some of them in fact then intensify 1–2 days later and even undergo rapid intensification such as ITC Bejisa in 2013, VITC Fantala in 2016, ITC Alcide in 2018, VITC Kenneth and TC Belna in 2019, all within 500 km radius NE of Madagascar.

For the other two regions, the number of TC-MHW days are much less (Tables 1 and 2) than NE Madagascar, but the percentage of intensification is about the same (~45%, Table 2, Fig. 7c) for south-central Mozambique and slightly lower for Comoros (~37%, Table 2, Fig. 7b). The latter region however shows 2 cases of rapid intensification after encountering a MHW, namely VITC Kenneth and TC Belna in 2019 (Fig. 7b). Although south-central Mozambique does not show any cases of rapid intensification during TC-MHW co-occurrences (Fig. 7c), TC Josie in 1997 and ITC Fanele in 2009 did rapidly intensify 1–2 days later after they passed over the MHW and while they were still within the 500 km box.

In south-central Mozambique, ITC Eline in February 2000 led to massive loss of life and devastation and intensified to Category-4 intensity just before it made landfall (Reason and Keibel, 2004). In this case, there was a pre-existing MHW, but it had ended a few days before landfall (although SSTs were still well above average). Further analysis showed that heat gain from the atmosphere (Fig. 8f) and a pre-existing barrier layer thickness (Fig. A3f) prior to the arrival of TC Eline pre-conditioned the surface and subsurface ocean (warmer subsurface ocean temperature, Fig. A2f) for TC intensification. As TC Eline tracked over this area, increased stratification, and stability within the water

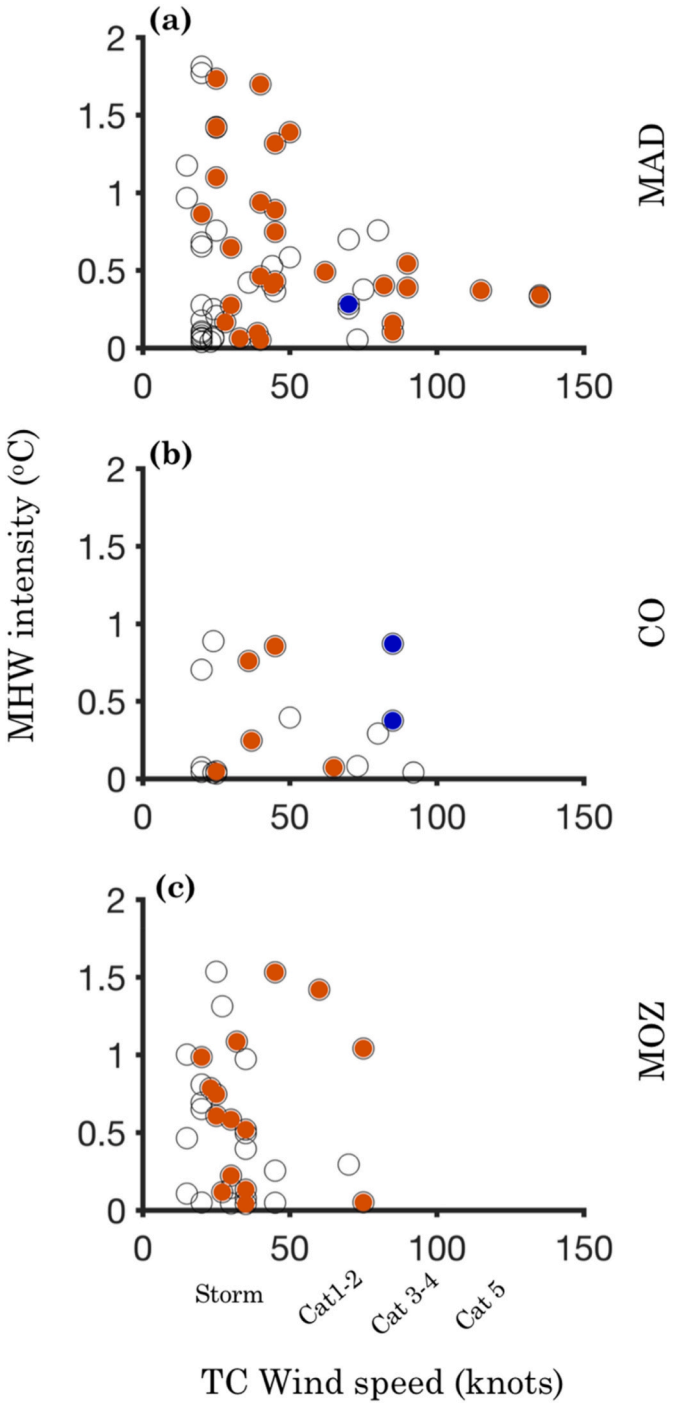

Fig. 7. TC-MHW co-occurrences (number of days when TC is within 500 km from MHW region and occur at the same time as MHW), where open circles highlight TCs (in days) that did not strengthen, orange dots are ones which strengthen (change in daily winds >0 knot), and blue dots are those that undergo rapid intensification (change in daily winds≥30 knots). Schematic diagram illustrates compounding processes. Distribution of all tropical cyclones (including tropical storms) and their associated daily wind speed (ms^{-1}; x axis) within 500 km from the centre of box (a) NE Madagascar (13.25–15.25°S; 50–52°E), (b) Comoros, (c) south-central Mozambique as a function of daily MHW intensity (°C; y axis) averaged in each coastal region from January 1982–December 2020. Wind speed with maximum sustained winds of 63 kts represent storms, and cyclones of Category 1–2 (maximum sustained winds of 64–89 kts), Category 3–4 (ITC, maximum sustained winds of 90–115 kts) and Category 5 (VITC, winds exceeding 115 kts) are illustrated. (For interpretation of the references to color in this figure legend, the reader is referred to the Web version of this article.)

Table 2
Statistics during TC-MHW co-occurrence: Percentage of TC days that co-occur with MHWs and percentage of TC-MHW cases that undergo TC Intensification in each coastal region, NE Madagascar, Comoros, and south-central Mozambique.

	NE Madagascar	Comoros	S Mozambique
% of TC days that encountered a MHW within 500 km from MHW region	13.8% (59 out of 426)	11.3% (19 out of 168)	13.3% (33 out of 248)
% TC-MHW co-occurrence (days) that showed intensification (change in daily winds >0)	47.5% (29 out of 59 days)	36.8% (7 out of 19 days)	45.4% (15 out of 33 days)
% of TCs that strengthened when they pass over MHWs	72.0% (18 out of 25 TCs)	55.5% (5 out of 9 TCs)	57.7% (8 out of 14 TCs)
Number of TCs that rapidly intensified (change in daily winds, RI≥30 knots) during TC-MHW	1 VITC Bansi (January 2015)	2 VITC Kenneth (April 2019) TC Belna (December 2019)	0

column acted as a barrier to entrainment cooling (weak/zero entrainment; Fig. A4f) and vertical mixing, which led to its intensification. Thus, the pre-existing strong MHW (Fig. 8f) induced by increased solar radiation (Fig. 8f), relaxation of winds (Fig. 8f) and reduced evaporative cooling (Fig. A4f), facilitated favourable subsurface conditions prior to TC Eline for its intensification.

There were substantially more MHW-TC co-occurrences during 2002–2021 than for the first two decades in the NE Madagascar and south-central Mozambique regions whereas for Comoros the numbers do not show any increasing tendency in the recent years (Figs. 4–6, A.1d-f). These results suggest that the warming climate in recent decades may be making TC-MHW co-occurrence more likely in at least some areas of the SWIO. Such warming then increases the upper ocean heat content and TCHP in the coastal zones considered thereby implying that when these TCs encounter a MHW event, they are more likely to intensify prior to landfall. In many cases, MHWs can be a preconditioning factor for TC intensification but for a TC to strengthen, both large-scale atmospheric conditions as well as the deeper ocean state also need to be favourable. Thus, the existence of a MHW cannot be taken on its own to imply that an approaching storm will intensify. Nevertheless, the fact that this has happened in many cases (Fig. 7, Table 2) highlights the need for increased understanding and real-time prediction of these potentially compounding events.

3.3.2. Role of TCs in weakening MHWs and associated coral reef thermal stress

While the previous section showed how a pre-existing MHW can often strengthen a TC passing over it, this section considers the impact of the TC on the MHW and associated coral reef thermal stress. Although the very strong winds, high sea state and turbulent upper ocean associated with TC passage can cause substantial mechanical damage to marine ecosystems, and particularly coral reefs, a potential benefit is that the TC may cool off pre-existing MHW in the upper ocean to cooler temperatures. Strong latent heat loss from the surface as well as vigorous mixing in the upper ocean together with entrainment of cooler subsurface waters into the mixed layer can all act to substantially reduce mixed layer temperatures, and thus weaken, or potentially end a pre-existing MHW once a TC has tracked past it. Out of the 25 TCs that co-occurred with MHWs NE of Madagascar, 80 (56) % of TCs weaken (end) the MHW following passage of the storm, while for Comoros the corresponding numbers are 100 (78) % of 9 TCs, and for south-central Mozambique, they are 72 (57) % of 14 TCs (Table 3).

Fig. 8 gives specific examples for each coastal zone of how the TC

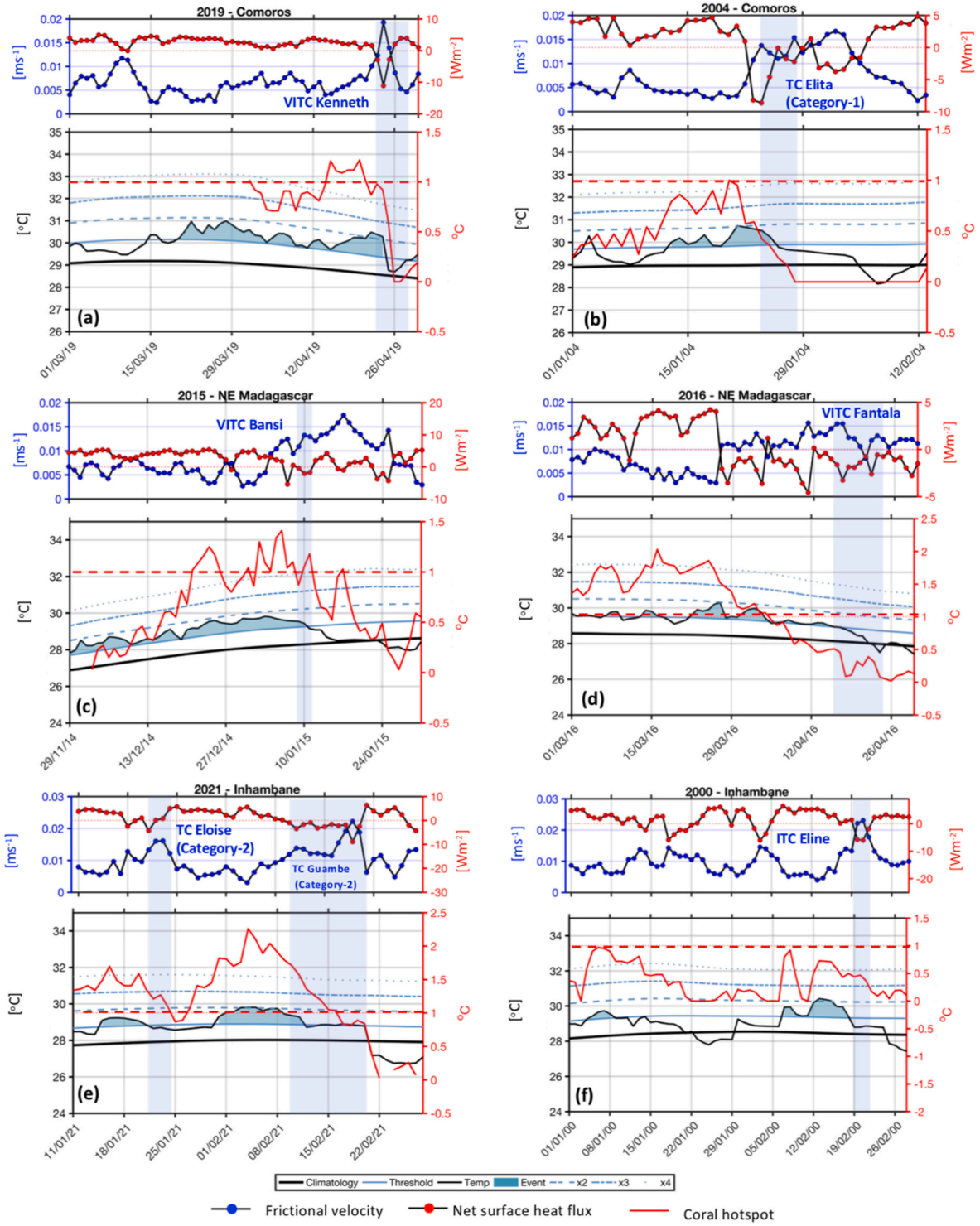

Fig. 8. Evolution of marine heatwaves in box NE Madagascar, Comoros and southern Mozambique coinciding with the passage of tropical cyclones within 500 km from the boxes: (a) Very Intense TC Kenneth in 2019, (b) TC Elita in 2004 near Comoros, (c) Very Intense TC Bansi in 2015, (d) Very Intense TC Fantala in 2016 near NE Madagascar, and (e) TC Eloise in 2021, TC Guambe in 2021, (f) Intense TC Eline in 2000 near southern Mozambique. Top panel shows the frictional velocity (ms^{-1}; in blue) and net surface heat flux (Wm^{-2}; in dotted red) calculated in each specific region. Bottom panel shows the evolution of the MHW, thick black and blue lines indicate MHW climatological mean and 90th percentile threshold respectively. MHW of Category 2–4 are represented by the dotted lines. The blue-shaded region indicates the MHW event detected using Hobday et al. (2016) definition. The evolution of coral hotspots at each virtual station (NE Madagascar, Comoros and Inhambane) is recorded for the same period (thick red line). Coral bleaching threshold is ≥1 °C (red dashed line). Vertical light blue shading indicates TC-MHW co-occurrence (i.e., when TC is within 500 km radial distance from the box). (For interpretation of the references to color in this figure legend, the reader is referred to the Web version of this article.)

Table 3
Statistics during TC-MHW co-occurrence: Percentage of TCs that contributed to the weakening and termination of MHWs in each coastal region, NE Madagascar, Comoros, and south-central Mozambique.

	NE Madagascar	Comoros	S Mozambique
% of TCs that weaken a MHW	80.0% (20 out of 25 TCs)	100.0% (9 out of 9 TCs)	71.7% (10 out of 14 TCs)
% of TCs that end a MHW	56.0% (14 out of 25 TCs)	77.8% (7 out of 9 TCs)	57.1% (8 out of 14 TCs)

impacts on a pre-existing MHW and coral bleaching event. Strong winds associated with TCs typically cool the upper ocean via increased evaporation, vertical mixing and pumping up of the thermocline driven by the cyclonic wind stress curl. The surface wind friction velocity provides a convenient metric to represent the TC impact on the upper ocean, as it is proportional to the amount of energy transferred from the atmosphere to the surface/subsurface ocean layer. In each case, it is clear that before the TC approached the coastal box, there was a net heat gain in the region, winds and hence the friction velocity were relatively weak, causing MHW and coral thermal stress conditions to persist. However, once the TC was sufficiently close as indicated by the vertical light blue shading (less than 500 km radial distance from the box), the associated wind friction velocity in the coastal box noticeably increased, causing a significant heat loss from the ocean to the atmosphere (Fig. 8) which led to a sharp drop off in coral thermal stress and weakening/termination of the MHW at each location. In most cases, the friction velocity associated with the cyclone exceeded 0.015 ms^{-1}. The energy uptake from the upper ocean by the TC cooled the temperature below the MHW criterion, halting the temperature trajectory towards coral bleaching.

To investigate the physical mechanism of the interaction between TCs and MHW, changes in the net surface heat flux (red dotted lines in Fig. 8) prior to, during and after TC-MHW co-occurrences were analysed in each coastal box. Besides the surface layers, the subsurface ocean also plays an important role in sustaining the MHW (through advection or entrainment) and tropical cyclone intensity. As such, the entrainment heat flux (Fig. A4), temperature response before and after the passage of the cyclone (Fig. A2), as well as barrier layer thickness (which provides stability of the water column; Fig. A3) were all analysed to better understand the role of stratification in the interaction between MHW and TCs.

Fig. 8a shows the case of Very Intense TC Kenneth approaching the Comoros in April 2019, which had previously been experiencing a prolonged period of above-average temperatures and thence a MHW that began over a month before Kenneth arrived. Increased net surface heat flux over the Comoros region before the passage of the cyclone, contributed to this strong and long-lasting MHW. As Kenneth tracked across the MHW region, it strengthened from tropical cyclone to intense tropical cyclone status with a large increase in wind friction velocity so that its energy uptake from the anomalously warm MHW in the upper ocean then quickly cooled the temperature below the coral bleaching threshold as well as ended the MHW. During the passage of Kenneth, intense mixing due to strong TC winds and reduced solar insolation (increased cloud cover and heat loss from ocean to atmosphere) resulted in a strong entrainment cooling (~−50 Wm^{-2}; Fig. A4a), a well-mixed and cooler water column (Fig. A2a), that led to the demise of the MHW. A few days after the passage of TC Kenneth, re-heating of the ocean surface (Fig. 8a) due to increased solar radiation and positive entrainment (detrainment; Fig. A4a) associated with a thin barrier layer led to stability of the water column (fresher water; Fig. A3a) which are favourable conditions for a re-emergence of the MHW.

In the second Comoros example (Fig. 8b), TC Elita was only a category-1 TC and did not intensify further due to the presence of cooler subsurface temperature anomalies prior to its passage (25–75 m deep, Fig. A2b). During TC-MHW co-occurrence, the strong stratification was disrupted (Fig. A2b), leading to a weak but positive entrainment (Fig. A4b) which made the cooling off less rapid, so after TC passage, the MHW ended more slowly than for Kenneth.

For NE Madagascar, Very Intense TC Bansi (Fig. 8c) occurred in January 2015, after an area of unusually warm ocean water developed earlier in the summer leading to a pre-existing MHW that lasted 4 months. The rate at which Bansi's friction velocities changed were less dramatic than for Kenneth and thus the reduction in the coral hotspot temperature below the bleaching threshold and the rate of MHW termination were much slower. The reduced surface and subsurface cooling (Fig. A2c) are due to a smaller heat loss to the atmosphere that often happens, presence of thin barrier layer (Fig. A3c) and no entrainment (Fig. A4c). In the case of Fantala in 2016 (Fig. 8d), the strongest TC ever recorded in the SWIO, the MHW and coral threshold had already started weakening before the TC arrived due to negative heat flux (Fig. 8d), but then dropped off further as the storm approached the NE Madagascar region as the friction velocities exceed 0.015 ms^{-1}. While Fantala itself may not have been the only contributor, hard coral in the region declined significantly from pre-bleaching levels of 28.5% in 2015 to 14.7% in 2017 (Gadoutsis et al., 2019).

For south-central Mozambique, Fig. 8e shows two examples for January–February 2021 when a pre-existing MHW was impacted by tropical cyclones, namely, TC Eloise and TC Guambe. The pre-existing MHW had started before Eloise arrived with SST well above the typical summer maximum, indicating strong to severe thermal stress on corals. As Eloise approached the MHW region, friction velocities increased rapidly leading to the termination of the MHW and decrease below the coral bleaching threshold. Fig. A4e shows strong entrainment cooling after Eloise reached its peak intensity on 24th January, but with the presence of a barrier layer prior to the passage of TC Eloise (Fig. A3e), a reduced subsurface cooling induced by the cyclone is observed (Figs. A2e, A3e). Following Eloise, the friction velocities quickly decreased enabling a stronger MHW to develop before TC Guambe occurred. Unlike TC Eloise which formed east of Madagascar before tracking into the Mozambique Channel, TC Guambe formed in the south-central channel itself close to the coastal zone considered here. This re-intensification of MHW in this region after the passage of TC Eloise could be attributed to a redistribution of upper ocean warming (Dzwonkowski et al., 2020) after the initial mixing by TC Eloise and the presence of the barrier layer on the 2nd February which transferred heat down to deeper portions (Figs. A2e, A3e). These processes allowed a re-warming of the water column, or a pre-conditioning to the formation of TC Guambe. As Guambe started to form, the increase in friction velocities was slower than for Eloise. With the presence of a thick barrier layer that contributed to the stability of the water column, the drop off in temperature was much slower and thus the MHW was able to persist longer than was the case after Eloise tracked over the previous MHW. Following the passage of TC Guambe, intense friction velocities in the region led to a drop of about −1.5 °C throughout the well-mixed water column due to strong heat loss (Fig. 8e) and entrainment cooling (Fig. A4e), ending the MHW there.

The other south-central Mozambique example (ITC Eline Fig. 8f) shows that the pre-existing MHW ended just before Eline arrived. Eline was a very large storm and the strong winds on its leading edge led to intense friction velocities, latent heat loss and upper ocean cooling. With the presence of a thick barrier layer after the passage of the cyclone (Fig. A3f), no entrainment cooling was observed (Fig. A4f), hence the existence of warmer subsurface layer (25–50 m deep) after passage of the storm (Fig. A2f).

In summary, this and the preceding sub-section (in particular Tables 2 and 3) have shown that a high percentage of pre-existing MHWs help strengthen TCs as they pass over the MHW region but that an even higher percentage of the TCs then weaken the MHW after passage of these storms.

4. Discussion

In recent years, countries bordering the Mozambique Channel have been severely impacted by a series of intense and devastating TCs, leading to flooding, wind damage and storm surges. This region is unique in Africa as being the only coastal zone on the continent experiencing tropical cyclone landfalls (note that TCs near West Africa, or hurricanes as they are known in the North Atlantic, track away from the continent towards the Caribbean). Strong cyclones can cause significant damage to coral reefs, particularly in cases where the reefs have previously been bleached by long periods of warming associated with MHWs. The three specific coastal zones focused on here (south-central Mozambique, northeastern Madagascar, and the Comoros islands) are highly prone to both TCs and MHWs and are also characterized by high biodiversity, including coral reefs and fisheries vital for the local economy both as a source of food and for supporting tourism. While TCs and MHWs have always been a characteristic of the climate of the coast in this part of Africa, there is evidence of recent increases in the frequency and intensity of severe tropical cyclones and long-lasting MHWs as the ocean warms with climate model projections indicating conditions are likely to worsen further in the near future (IPCC et al., 2013; 2021). Thus, coastal communities in Mozambique, Madagascar and neighbouring islands need to adapt further to reduce the severe impacts of these coastal hazards on their livelihoods (Hahn et al., 2009; Osbahr et al., 2010; Artur and Hilhorst, 2012).

Of the three coastal zones studied here, northeastern Madagascar is more frequently impacted by landfalling cyclones with a greater percentage of its annual rainfall coming from these systems than is south-central Mozambique and Comoros. Although there is a significantly increasing trend in tropical cyclone heat potential (TCHP) in all three coastal areas, a faster rate is observed northeast of Madagascar, suggesting that tropical cyclones are more likely to intensify further here as they approach this coast. More generally, a significantly increasing tendency in the number of severe TCs has been observed west of 90°E in the SWIO (Malan et al., 2013). Although TCs are less common in south-central Mozambique than Madagascar, this coast has been severely affected by nearby landfalling severe cyclones during exceptional summer seasons such as Idai in March 2019 or Eline in February 2000 with associated very large loss of life and damage. The likelihood of an actual landfall in Comoros is necessarily less as these islands are very small in area but cyclones can track very close such as Very Intense TC Kenneth in April 2019.

MHW frequency and duration are also significantly increasing in all three coastal boxes but with a faster rate in northeastern Madagascar and south-central Mozambique than Comoros, both annually and for the summer. Since prolonged MHW events lead to coral bleaching and devastate local fish stocks, the increasing trend has serious implications for coastal communities here. For coral bleaching, the results also showed a statistically increasing trend in each coastal region, again faster northeast of Madagascar with several particularly strong cases in 1998, 2010, 2016 and 2021, some of which coincide with El Niño years. Therefore, the ability to forecast MHWs in coastal areas can reduce coral recovery times by extending the time available to implement ways to mitigate local scale stress from human-related activities at severely impacted sites, such as restrictions of fishing or tourism activities.

Co-occurring MHW and TC events lead to damage on coastal ecosystems being compounded compared to cases when these events occur separately. For instance, severe cyclones Ockhi in 2017 and Fani in 2019 in the North Indian Ocean, underwent sudden and rapid intensification after encountering warm ocean anomalies (Singh et al., 2020, 2021), which in turn led to a considerable socio-economic impact in India due to the country's densely populated coastal areas. Although these studies do not identify the warm ocean anomalies as MHWs, the online marine heatwave tracker tool (Schlegel, 2020) detected the presence of MHWs along the paths of severe cyclones Ockhi and Fani suggesting that some of the results reported here for the SWIO may also have relevance for the coast of India. In the SWIO region, TC-MHW co-occurrences have happened more often in the recent decade than in the 1982–2001 period. Parameter-space plots show that for each coastal region, pre-existing MHWs may provide a pre-conditioning effect for TCs approaching the coast. 72% of co-occurring TCs and MHWs northeast of Madagascar undergo intensification, with slightly lower percentages in the other two regions. On the other hand, an even higher percentage of TCs tend to weaken or even terminate MHW events along their paths. The parameter-space plot may then be a useful way in which to categorize and monitor the co-occurrence of these coastal high impact events not just in southeastern Africa but potentially other parts of the world prone to TCs impacting the coastal zone.

Case studies of intense TCs in each coastal region show that before the arrival of a TC, winds and friction velocity were relatively weak, intense heat gain prevailed over the region, sustaining MHWs and thermal stresses above the coral bleaching threshold. However, once the TC leads to sufficient increases in wind friction velocity, a sharp decrease in coral thermal stress and weakening/termination of the MHW occurs. Intense mixing due to strong TC winds and reduced solar insolation (increased cloud cover and heat loss from ocean to atmosphere) resulted in a strong entrainment cooling, a well-mixed and cooler water column, that led to weakening and sometimes the demise of the MHW. In a few cases, the presence of a thick barrier layer prior to TC-MHW co-occurrence may provide stability within the water column and act as a barrier to entrainment cooling which may lead to a re-emergence of the MHW. Recent studies (Rathore et al., 2022; Chatterjee et al., 2022) in the Bay of Bengal and Arabian Sea have also shown that extreme events in the ocean and atmosphere can interact with each other (whereby the MHW intensifies the tropical cyclone, and the tropical cyclone dissipates the MHW) and can both generate a compound extreme event, causing severe socio-economic consequences. Such co-occurrences are likely to be important in other TC prone coastal areas like the Caribbean, southeastern coast of the US, tropical Australia, and south and east Asia.

Many seasons will experience damaging MHWs without a co-occurring TC. It is therefore important to note that less stormy summers are not necessarily more favourable for reduced thermal stresses on coral and other marine ecosystems than those which experience more strong cyclones. On the other hand, given that SST is generally always above 26 °C in summer in this region, TCs can often impact the coastal zone without a MHW event already occurring.

5. Conclusion

This study examined the characteristics of two severe types of coastal hazards, tropical cyclones and marine heat waves, impacting the coast of southeastern Africa as well as the ways in which they may interact with each other. Northeastern Madagascar appears to be the more prone to these highly damaging adverse events than does south-central Mozambique or the Comoros Islands. However, the long-term warming of the SWIO and increase in severe tropical cyclone days together with climate model projections suggests that most parts of southeastern Africa are likely to face increasing hazardous impacts in the future. While there were noticeable improvements in warning systems in Mozambique following the landfall of intense Tropical Cyclone Eline in 2000 and its associated heavy loss of life, coastal communities here and elsewhere in the region remain very vulnerable to high impact weather events. Future work should therefore focus on improving the forecasting, warning and mitigation of these coastal hazards as well as exploring in more detail the processes by which they may interact with each other and compound their impacts. Since temperature extremes on the continental shelf can extend far deeper than the mixed layer, more research on the vertical structure of MHWs is needed particularly in these coastal areas where the marine ecosystem is already under threat. A significant challenge to such work remains the relative lack of sufficiently high quality observations in southeastern Africa compared to other tropical cyclone regions in the world. However, our study has

highlighted the complex relationships between these devastating coastal hazards in southeastern Africa with the view to raising awareness for the need for improved real time observing systems to support this highly vulnerable region in both forecasting and mitigating climate change impacts.

CRediT authorship contribution statement

D. Mawren: Conceptualization, Data curation, Formal analysis, Investigation, Methodology, Software, Visualization, Writing – original draft. **J. Hermes:** Funding acquisition, Resources, Supervision, Validation, Writing – review & editing. **C.J.C. Reason:** Conceptualization, Funding acquisition, Project administration, Resources, Supervision, Validation, Writing – review & editing.

Declaration of competing interest

The authors declare that they have no known competing financial interests or personal relationships that could have appeared to influence the work reported in this paper.

Data availability

Data are freely available.

Acknowledgements

The research leading to these results has received funding from the National Research Foundation (NRF) ACSyS grant 114690, University of Cape Town Science Faculty Fellowship to the first author and the South African Environmental Observation Network (SAEON). The authors are grateful to ECMWF (https://cds.climate.copernicus.eu/cdsapp#!/dataset/reanalysis-era5-single-levels?tab=form), Climate Hazards Group InfraRed Precipitation with Station Data (CHIRPS; https://www.chc.ucsb.edu/data/chirps), the International Best Track Archive for Climate Stewardship (IBTrACS) data set (https://www.ncei.noaa.gov/data/international-best-track-archive-for-climate-stewardship-ibtracs/v04r00/access/netcdf/), NOAA's Optimum Interpolation Sea Surface temperature (OISST) and GLORYS12V1 product (https://resources.marine.copernicus.eu/?option=com_csw&view=order&record_id=c0635fc4-07d3-4309-9d55-cfd3e6aa788b) for making satellite, ocean model, and atmospheric reanalysis data freely available. We also thank two reviewers whose constructive comments helped to greatly improve this manuscript.

Appendix A. Supplementary data

Supplementary data to this article can be found online at https://doi.org/10.1016/j.ecss.2022.108056.

References

Amone-Mabuto, M., Bandeira, S., da Silva, A., 2017. Long-term changes in seagrass coverage and potential links to climate-related factors: the case of Inhambane Bay, southern Mozambique. West. Indian Ocean J. Mar. Sci. 16 (2), 13–25.

Arndt, C., Strzepeck, K., Tarp, F., Thurlow, J., Fant, C., Wright, L., 2010. Adapting to climate change: an integrated biophysical and economic assessment for Mozambique". Sustain. Sci. 6 (1), 7–20. https://doi.org/10.1007/s11625-010-0118-9.

Artur, L., Hilhorst, D., 2012. Everyday realities of climate change adaptation in Mozambique". Global Environ. Change 22 (2), 529–536. https://doi.org/10.1016/j.gloenvcha.2011.11.013.

Backeberg, B.C., Reason, C.J.C., 2010. A connection between the south equatorial current north of Madagascar and Mozambique channel eddies. Geophys. Res. Lett. 37 (4), L04604 https://doi.org/10.1029/2009GL041950.

Balaguru, K., Chang, P., Saravanan, R., Leung, L.R., Xu, Z., Li, M., Hsieh, J.S., 2012. Ocean barrier layers' effect on tropical cyclone intensification. Proc. Natl. Acad. Sci. USA 109 (36), 14343–14347. https://doi.org/10.1073/pnas.1201364109.

Banzon, V., Smith, T.M., Chin, T.M., Liu, C., Hankins, W., 2016. A long-term record of blended satellite and in situ sea-surface temperature for climate monitoring, modeling and environmental studies. Earth Syst. Sci. Data 8 (1), 165–176. https://doi.org/10.5194/essd-8-165-2016.

Blamey, R.C., Kolusu, S.R., Mahlalela, P., Todd, M.C., Reason, C.J.C., 2018. The role of regional circulation features in regulating El Nino climate impacts over southern Africa: a comparison of the 2015/2016 drought with previous events. Int. J. Climatol. 38, 4276–4295. https://doi.org/10.1002/joc.5668.

Cavole, L., et al., 2016. Biological impacts of the 2013–2015 warm-water anomaly in the Northeast Pacific: winners, losers, and the future. Oceanography 29, 273–285. https://doi:10.5670/oceanog.2016.32.

Chatterjee, A., Anil, G., Shenoy, L.R., 2022. Marine heatwaves in the Arabian Sea. Ocean Sci. 18 (3), 639–657. https://doi.org/10.5194/os-18-639-2022.

de Boyer Montégut, C., Madec, G., Fischer, A.S., Lazar, A., Iudicone, D., 2004. Mixed layer depth over the global ocean: an examination of profile data and a profile-based climatology. J. Geophys. Res.: Oceans 109 (C12). https://doi.org/10.1029/2004JC002378.

Department of Forestry, 2021. Fisheries, and the Environment. March 7). *East coast marine heatwave and large fish and shellfish washout* [Press release]. https://www.environment.gov.za/mediarelease/heatwaveandfishwalkout_eastcoastmarine.

Dzwonkowski, B., Coogan, J., Fournier, S., Lockridge, G., Park, K., Lee, T., 2020. Compounding impact of severe weather events fuels marine heatwave in the coastal ocean. Nat. Commun. 11 (1), 1–10. https://doi.org/10.1038/s41467-020-18339-2.

Eckstein, D., Künzel, V., Schäfer, L., 2021. Global Climate Risk Index 2021. *Who Suffers Most from Extreme Weather Events*, pp. 2000–2019.

Eriksson, H., Wickel, J., Jamon, A., 2012. Coral bleaching and associated mortality in Mayotte, Western Indian Ocean. West. Indian Ocean J. Mar. Sci. 11 (1), 113–118.

Foltz, G.R., Vialard, J., Praveen Kumar, B., McPhaden, M.J., 2010. Seasonal mixed layer heat balance of the southwestern tropical Indian Ocean. J. Clim. 23 (4), 947–965. https://doi.org/10.1175/2009JCLI3268.1.

Funk, C.C., Peterson, P.J., Landsfeld, M.F., Pedreros, D.H., Verdin, J.P., Rowland, J.D., et al., 2014. A quasi-global precipitation time series for drought monitoring. US Geological Survey data series 832 (4), 1–12. https://doi.org/10.3133/ds832.

Gadoutsis, E., Daly, C.A., Hawkins, J.P., Daly, R., 2019. Post-bleaching mortality of a remote coral reef community in Seychelles, Western Indian Ocean. West. Indian Ocean J. Mar. Sci. 18 (1), 11–18. https://doi.org/10.4314/wiojms.v18i1.2.

Gao, X., Li, G., Liu, J., Long, S.M., 2022. The trend and interannual variability of marine heatwaves over the bay of Bengal. Atmosphere 13 (3), 469. https://doi.org/10.3390/atmos13030469.

George, R., 2019. *Seagrasses in Warming Oceans: Physiological and Biogeochemical Responses* (Doctoral Dissertation. Department of Ecology, Environment and Plant Sciences, Stockholm University.

Gimeno, L., Dominguez, F., Nieto, R., Trigo, R., Drumond, A., Reason, C.J., et al., 2016. Major Mechanisms of Atmospheric Moisture Transport and Their Role in Extreme Precipitation Events. http://drs.nio.org/drs/handle/2264/5046.

Graham, N.A., Wilson, S.K., Jennings, S., Polunin, N.V., Bijoux, J.P., Robinson, J., 2006. Dynamic fragility of oceanic coral reef ecosystems. Proc. Natl. Acad. Sci. USA 103 (22), 8425–8429. https://doi.org/10.1073/pnas.0600693103.

Hahn, M.B., Riederer, A.M., Foster, S.O., 2009. The livelihoods vulnerability index: a pragmatic approach to assessing risks from climate variability and change – a case study in Mozambique". Global Environ. Change 19 (1), 74–88. https://doi.org/10.1016/j.gloenvcha.2008.11.002.

Halo, I., Backeberg, B., Penven, P., Ansorge, I., Reason, C., Ullgren, J.E., 2014. Eddy properties in the Mozambique Channel: a comparison between observations and two numerical ocean circulation models. Deep Sea Res. Part II Top. Stud. Oceanogr. 100, 38–53. https://doi.org/10.1016/j.dsr2.2013.10.015.

Hobday, A.J., Alexander, L.V., Perkins, S.E., Smale, D.A., Straub, S.C., Oliver, E.C., et al., 2016. A hierarchical approach to defining marine heatwaves. Prog. Oceanogr. 141, 227–238. https://doi.org/10.1016/j.pocean.2015.12.014.

Hobday, A.J., Oliver, E.C., Gupta, A.S., Benthuysen, J.A., Burrows, M.T., Donat, M.G., et al., 2018. Categorizing and naming marine heatwaves. Oceanography 31 (2), 162–173.

Hughes, T.P., Baird, A.H., Bellwood, D.R., Card, M., Connolly, S.R., Folke, C., et al., 2003. Climate change, human impacts, and the resilience of coral reefs. Science 301 (5635), 929–933. https://doi.org/10.1126/science.1085046.

INGC, 2009. Study on the impact of climate change on disaster risk in Mozambique: synthesis report – first draft". available at: www.irinnews.org/pdf/synthesis_report_final_draft_march09.pdf.

IPCC Climate Change 2013, Stocker, T.F., Qin, D., Plattner, G.K., Tignor, M., Allen, S.K., Boschung, J., et al., 2013. In: 2013. Climate Change 2013: the Physical Science Basis. *Contribution Of Working Group I to the Fifth Assessment Report of the Intergovernmental Panel on Climate Change*, p. 1535.

IPCC, 2021. Summary for policymakers. In: Zhai, P., Pirani, A., Connors, S.L., Péan, C., Berger, S., Caud, N., Chen, Y., Goldfarb, L., Gomis, M.I., Huang, M., Leitzell, K., Lonnoy, E., Matthews, J.B.R., Maycock, T.K., Waterfield, T., Yelekçi, O., Yu, R., Zhou, B. (Eds.), Climate Change 2021: the Physical Science Basis. Contribution of Working Group I to the Sixth Assessment Report of the Intergovernmental Panel on Climate Change [Masson-Delmotte, V. Cambridge University Press (in press).

Jiang, H., Liu, C., Zipser, E.J., 2011. A TRMM-based tropical cyclone cloud and precipitation feature database. J. Appl. Meteorol. Climatol. 50 (6), 1255–1274. https://doi.org/10.1175/2011JAMC2662.1.

Kaplan, J., DeMaria, M., 2003. Large-scale characteristics of rapidly intensifying tropical cyclones in the North Atlantic basin. Weather Forecast. 18 (6), 1093–1108. https://doi.org/10.1175/1520-0434(2003)018<1093:LCORIT>2.0.CO;2.

Klinman, M., Reason, C.J.C., 2008. On the peculiar storm track of TC Favio during the 2006-2007 South West Indian Ocean tropical cyclone season and relationships to ENSO. Met. Atmos. Phys. 100, 233–242. https://doi.org/10.1007/s00703-008-0306-7.

Knapp, K.R., Kruk, M.C., Levinson, D.H., Diamond, H.J., Neumann, C.J., 2010. The international best track archive for climate stewardship (IBTrACS) unifying tropical cyclone data. Bull. Am. Meteorol. Soc. 91 (3), 363–376. https://doi.org/10.1175/2009BAMS2755.1.

Knapp, K.R., Velden, C.S., Wimmers, A.J., 2018. A global climatology of tropical cyclone eyes. Mon. Weather Rev. 146 (7), 2089–2101. https://doi.org/10.1175/MWR-D-17-0343.1.

Larson, J., Zhou, Y., Higgins, R.W., 2005. Characteristics of landfalling tropical cyclones in the United States and Mexico: climatology and interannual variability. J. Clim. 18 (8), 1247–1262. https://doi.org/10.1175/JCLI3317.1.

Lin, I.I., Goni, G.J., Knaff, J.A., Forbes, C., Ali, M.M., 2013. Ocean heat content for tropical cyclone intensity forecasting and its impact on storm surge. Nat. Hazards 66 (3), 1481–1500. https://doi.org/10.1007/s11069-012-0214-5.

Lutjeharms, J.R., 2006. The Agulhas Current, 329. Springer, Berlin. https://doi.org/10.1007/3-540-37212-1.

Malan, N., Reason, C.J.C., Loveday, B.R., 2013. Variability in tropical cyclone heat potential over the Southwest Indian Ocean. J. Geophys. Res.: Oceans 118 (12), 6734–6746. https://doi.org/10.1002/2013JC008958.

Matyas, C.J., 2013. Processes influencing rain-field growth and decay after tropical cyclone landfall in the United States. J. Appl. Meteorol. Climatol. 52 (5), 1085–1096. https://doi.org/10.1175/JAMC-D-12-0153.1.

Matyas, C.J., 2014. Conditions associated with large rain-field areas for tropical cyclones landfalling over Florida. Phys. Geogr. 35 (2), 93–106. https://doi.org/10.1080/02723646.2014.893476.

Mavume, A.F., Rydberg, L., Rouault, M., Lutjeharms, J.R., 2009. Climatology and landfall of tropical cyclones in the south-west Indian Ocean. West. Indian Ocean J. Mar. Sci. 8 (1), 15–36. https://doi.org/10.4314/wiojms.v8i1.56672.

Mawren, D., Reason, C.J.C., 2017. Variability of upper-ocean characteristics and tropical cyclones in the South West Indian Ocean. J. Geophys. Res.: Oceans 122 (3), 2012–2028. https://doi.org/10.1002/2016JC012028.

Mawren, D., Hermes, J., Reason, C.J.C., 2020. Exceptional tropical cyclone Kenneth in the far northern Mozambique Channel and ocean eddy influences. Geophys. Res. Lett. 47 (16), e2020GL088715 https://doi.org/10.1029/2020GL088715.

Mawren, D., Hermes, J., Reason, C.J.C., 2021. Marine heatwaves in the Mozambique channel. Clim. Dynam. 58 (1), 305–327. https://doi.org/10.1007/s00382-021-05909-3.

Mawren, D., Blamey, R., Hermes, J., Reason, C.J.C., 2022. On the importance of the Mozambique Channel for the climate of southeastern Africa. Clim. Dynam. 1–21. https://doi.org/10.1007/s00382-022-06334-w.

Mikaelyan, A.S., Zatsepin, A.G., Kubryakov, A.A., 2020. Effect of mesoscale eddy dynamics on bioproductivity of the marine ecosystems. Phys. Oceanogr. 27 (6), 590–618.

Mills, K.E., Pershing, A.J., Brown, C.J., Chen, Y., Chiang, F.S., Holland, D.S., et al., 2013. Fisheries management in a changing climate: lessons from the 2012 ocean heat wave in the Northwest Atlantic. Oceanography 26 (2), 191–195.

Morake, D.M., Blamey, R.C., Reason, C.J.C., 2021. Long-lived mesoscale convective systems over eastern South Africa. J. Clim. 34 (15), 6421–6439. https://doi.org/10.1175/JCLI-D-20-0851.1.

Mukwenha, S., Dzinamarira, T., Chingombe, I., Mapingure, M.P., Musuka, G., 2021. Health emergency and disaster risk management: a case of Zimbabwe's preparedness and response to cyclones and tropical storms: We are not there yet. Public Health in Practice 2, 100131.

Niiler, P.P., 1977. One-dimensional models of the upper ocean. Modelling and Prediction of the Upper Layers of the Ocean 143–172.

NOAA Coral Reef Watch, 2018. *NOAA Coral Reef Watch Version 3.1 Daily Global 5km Satellite Coral Bleaching HotSpot Product*, Jan. 1, 1986-Dec. 31, 2020. NOAA Coral Reef Watch. Data set, College Park, Maryland, USA updated daily. 2022-06-13 at ftp:ftp.star.nesdis.noaa.gov/pub/sod/mecb/crw/data/5km/v3.1_op/nc/v1.0/daily/hs/.

Obura, D., 2012. The diversity and biogeography of Western Indian Ocean reef-building corals. PLoS One 7, e45013. https://doi:10.1371/journal.pone.0045013.

Obura, D.O., Church, J.E., Gabrie, C., 2012. Assessing Marine World Heritage Form an Ecosystem Perspective: the Western Indian Ocean. World Heritage Centre, United Nations Education, Science and Cultural Organization (UNESCO), p. 124.

Obura, D., et al., 2017. Reviving the Western Indian Ocean Economy: Actions for a Sustainable Future. WWF International, Gland, Switzerland, p. 64.

Obura, D.O., Bigot, L., Benzoni, F., 2018. Coral responses to a repeat bleaching event in Mayotte in 2010. PeerJ 6, e5305. https://doi.org/10.7717/peerj.5305.

Oliver, E.C., Benthuysen, J.A., Bindof, N.L., Hobday, A.J., Holbrook, N.J., Mundy, C.N., Perkins-Kirkpatrick, S.E., 2017. The unprecedented 2015/16 Tasman Sea marine heatwave. Nat. Commun. 8 (1), 1–12. https://doi.org/10.1038/ncomms16101.

Oliver, E.C., Lago, V., Hobday, A.J., Holbrook, N.J., Ling, S.D., Mundy, C.N., 2018. Marine heatwaves of eastern Tasmania: trends, interannual variability, and predictability. Prog. Oceanogr. 161, 116–130. https://doi.org/10.1016/j.pocean.2018.02.007.

Oliver, E.C., Burrows, M.T., Donat, M.G., Sen Gupta, A., Alexander, L.V., Perkins-Kirkpatrick, S.E., et al., 2019. Projected marine heatwaves in the 21st century and the potential for ecological impact. Front. Mar. Sci. 6, 734. https://doi.org/10.3389/fmars.2019.00734.

Oliver, E.C., Benthuysen, J.A., Darmaraki, S., Donat, M.G., Hobday, A.J., Holbrook, N.J., et al., 2021. Marine heatwaves. Ann. Rev. Mar. Sci 13, 313–342.

Osbahr, H., Twyman, C., Adger, W.N., Thomas, D.S.G., 2010. Evaluating successful livelihood adaptation to climate variability and change in Southern Africa". Ecol. Soc. 15 (2), 27 available at: www.ecologyandsociety.org/vol15/iss2/art27/.

Paling, E.I., Kobryn, H.T., Humphreys, G., 2008. Assessing the extent of mangrove change caused by Cyclone Vance in the eastern Exmouth Gulf, northwestern Australia. Estuar. Coast Shelf Sci. 77, 603–613. https://doi.org/10.1016/j.ecss.2007.10.019.

Pereira, M.A.M., Litula, C., Santos, R., Leal, M., Fernandes, R.S., Tibibiçá, Y., Williams, J., Atanassov, B., Carreira, F., Massingue, A., Marques da Silva, I., 2014. Mozambique Marine Ecosystems Review.

Pielke, R.A., 2013. The Hurricane. Routledge, p. 240. https://doi.org/10.4324/9781315822679.

Rathore, S., Goyal, R., Jangir, B., Ummenhofer, C.C., Feng, M., Mishra, M., 2022. Interactions between a marine heatwave and tropical cyclone Amphan in the bay of Bengal in 2020. Front. Clim. 4, 861477. https://doi:10.3389/fclim.2022.861477.

Reason, C.J.C., Allan, R.J., Lindesay, J.A., Ansell, T.J., 2000. ENSO and climatic signals across the Indian Ocean basin in the global context: Part I, Interannual composite patterns. Int. J. Climatol.: A Journal of the Royal Meteorological Society 20 (11), 1285–1327. https://doi.org/10.1002/1097-0088(200009)20:11<1285::AID-JOC536>3.0.CO;2-R.

Reason, C.J.C., Keibel, A., 2004. Tropical cyclone Eline and its unusual penetration and impacts over the southern African mainland. Weather Forecast. 19 (5), 789–805. https://doi.org/10.1175/1520-0434(2004)019<0789:TCEAIU>2.0.CO;2.

Ridderinkhof, W., Le Bars, D., Von der Heydt, A.S., De Ruijter, W.P.M., 2013. Dipoles of the south east Madagascar current. Geophys. Res. Lett. 40 (3), 558–562.

Sadhuram, Y., Maneesha, K., Murty, T.R., 2010. Importance of upper ocean heat content in the intensification and translation speed of cyclones over the Bay of Bengal. Curr. Sci. 99 (9), 1191–1194.

Saranya, J.S., Roxy, M.K., Dasgupta, P., Anand, A., 2022. Genesis and trends in marine heatwaves over the tropical Indian Ocean and their interaction with the Indian summer monsoon. J. Geophys. Res.: Oceans 127 (2), e2021JC017427. https://doi.org/10.1029/2021JC017427.

Schlegel, R.W., Oliver, E.C., Wernberg, T., Smit, A.J., 2017. Nearshore and offshore co-occurrence of marine heatwaves and cold-spells. Prog. Oceanogr. 151, 189–205. https://doi.org/10.1016/j.pocean.2017.01.004.

Schlegel, R.W., 2020. Marine Heatwave Tracker. https://doi.org/10.5281/zenodo.3787872. http://www.marineheatwaves.org/tracker.

Shay, L.K., Goni, G.J., Black, P.G., 2000. Effects of a warm oceanic feature on Hurricane Opal. Mon. Weather Rev. 128, 1366–1383. https://doi.org/10.1175/1520-0493(2000)128<1366:EOAWOF>2.0.CO;2.

Sheppard, C.R., 2003. Predicted recurrences of mass coral mortality in the Indian Ocean. Nature 425 (6955), 294–297. https://doi.org/10.1038/nature01987.

Singh, V.K., Roxy, M.K., Deshpande, M., 2020. The unusual long track and rapid intensification of very severe cyclone Ockhi. Curr. Sci. 119 (5), 771–779.

Singh, V.K., Roxy, M.K., Deshpande, M., 2021. Role of warm ocean conditions and the MJO in the genesis and intensification of extremely severe cyclone Fani. Sci. Rep. 11 (1), 1–10.

Singleton, A.T., Reason, C.J.C., 2006. Numerical simulations of a severe rainfall event over the Eastern Cape coast of South Africa: sensitivity to sea surface temperature and topography. Tellus Dyn. Meteorol. Oceanogr. 58 (3), 335–367. https://doi.org/10.1111/j.1600-0870.2006.00180.x.

UNEP-WCMC, , WorldFish Centre, WRI, T.N.C., 2018. Global distribution of coral reefs, compiled from multiple sources including the Millennium Coral Reef Mapping Project. Version 4.0, updated by UNEP-WCMC. Includes contributions from IMaRSUSF and IRD (2005), IMaRS-USF (2005) and Spalding et al. (2001). UNEP World Conservation Monitoring Centre, Cambridge (UK). URL: http://data.unepwcmc.org/datasets/1. (Accessed 13 July 2022).

Wada, A., Usui, N., 2007. Importance of tropical cyclone heat potential for tropical cyclone intensity and intensification in the western North Pacific. J. Oceanogr. 63 (3), 427–447. https://doi.org/10.1007/s10872-007-0039-0.

Walker Jr., H.J., Hastings, P.A., Hyde, J.R., Lea, R.N., Snodgrass, O.E., Bellquist, L.F., 2020. Unusual occurrences of fishes in the Southern California Current System during the warm water period of 2014–2018. Estuar. Coast Shelf Sci. 236, 106634 https://doi.org/10.1016/j.ecss.2020.106634.

Wang, X., Han, G., Qi, Y., Li, W., 2011. Impact of barrier layer on typhoon-induced sea surface cooling. Dynam. Atmos. Oceans 52 (3), 367–385. https://doi.org/10.1016/j.dynatmoce.2011.05.002.

WFP, 2021. Food Security and Livelihoods under a Changing Climate in Mozambique.

Wilson, S.K., Graham, N.A., Pratchett, M.S., Jones, G.P., Polunin, N.V., 2006. Multiple disturbances and the global degradation of coral reefs: are reef fishes at risk or resilient? Global Change Biol. 12 (11), 2220–2234. https://doi.org/10.1111/j.1365-2486.2006.01252.x.

World Bank, 2017. Mozambique Country Forest Note. © World Bank. http://documents1.worldbank.org/curated/en/693491530168545091/pdf/Mozambique-Country-Forest-Note.pdf.

World Bank, 2020. Madagascar: Balancing Conservation and Exploitation of Fisheries Resources. https://www.worldbank.org/en/news/feature/2020/06/08/madagascar-balancing-conservation-and-exploitation-of-fisheries-resources.